Palacký University Olomouc
Faculty of Natural Sciences
Department of Optics

Polarization and spatial hyper-encoding for quantum logic gates

Diploma thesis

Bc. Robert Čerňanský

Author:	Robert Čerňanský
Study program:	N1701 Fyzika
Field of study:	1701T029 Optika a Optoelektronika
Form of study:	Prezenční
Supervisor:	Mgr. Michal Mičuda Ph.D.
Co-supervisor:	Mgr. Miroslav Ježek Ph.D.
Date of turning:	30.4.2015

Univerzita Palackého v Olomouci
Přírodovědecká fakulta
Katedra optiky

Polarizační a prostorové hyper kódováni pro kvantová logická hradla

Diplomová práce

Bc. Robert Čerňanský

Autor:	Robert Čerňanský
Studijní program:	N1701 Fyzika
Studijní obor:	1701T029 Optika a Optoelektronika
Forma studia:	Prezenční
Vedoucí práce:	Mgr. Michal Mičuda Ph.D.
Konzultant:	Mgr. Miroslav Ježek Ph.D.
Termín odevzdání práce:	30.4.2015

Prohlašuji, že jsem předloženou diplomovou práci vypracoval samostatně pod vedením Mgr. Michal Mičuda Ph.D a že jsem použil zdrojů, které cituji a uvádím v seznamu použitých pramenů.

V Olomouci ……. ...…….....

Bibliografická identifikace:

Jméno a příjmení autora	Robert Čerňanský
Název práce	Polarizačné a priestorové hyper kódovanie pre kvantové logické hradla
Typ práce	Diplomová
Pracoviště	Katedra optiky
Vedoucí práce	Mgr. Michal Mičuda Ph.D.
Konzultant	Mgr. Miroslav Ježek Ph.D.
Rok obhajoby práce	2015
Abstrakt	Cieľom práce je zostavenie experimentu, ktorý využíva polarizačný interferometer. Budeme realizovať konvertor ktorý zabezpečuje prechod medzi priestorovým a polarizačným módom svetla, ľaditelný polarizačný filter a zariadenie schopné hyperkódovať informácie do polarizačného a zároveň priestorového módu svetla. Zariadenia budeme charakterizovať pomocou priamej rekonštrukcie a pomocou tomografickej metódy maximum likelihood.
Klíčová slova	Polarizačné kódovanie, dráhové kódovanie, kvantová rekonštrukcia stavu, priama metóda, metóda Maximum likelihood, rekonštrukcia kvantového procesu, fidelita procesu
Počet stran	46
Počet příloh	4
Jazyk	Anglický

Bibliographical identification:

Autor's first name and surname	Robert Čerňanský
Title	Polarization and spatial hyper-encoding for quantum logic gates
Type of thesis	Master
Department	Department of Optics
Supervisor	Mgr. Michal Mičuda Ph.D.
Consultant	Mgr. Miroslav Ježek Ph.D.
The year of presentation	2015
Abstract	The aim of the thesis deals with building an experimental setups using polarization interferometer. We will realize convertor between spatial and polarization mode of light, tunable polarization filter and device capable of hyper-encoding of information into polarization and spatial mode of light simultaneously. Devices will be characterized by full tomography using linear inversion and maximum likelihood method.
Keywords	Polarisation coding, spatial coding, state reconstruction, linear inversion method, maximum likelihood method, process reconstruction, process fidelity
Number of pages	46
Number of appendices	4
Language	English

Contents

Introduction **7**

1 Chapter 1: Theory **8**

1.1 Polarization....8
1.2 Jones Formalism....8
1.3 Stokes Formalism....10
1.4 Interference of two partially coherent waves....12
1.5 One qubit tomography and polarization state reconstruction....12
1.6 Maximum likelihood reconstruction method....13
1.7 Reconstruction of process matrix (completely positive CP map)...14

2 Chapter 2: Experiment **17**

2.1 Converter between polarization and spatial modes....17
2.2 Preparation of MZ interferometer for hyper-encoding....24
2.3 Partially tunable polarization filter....33
2.4 Polarization and spatial hyper-encoding....40

3 Chapter 3: Conclusion **47**

Appendix **48**

Refferences **51**

Introduction

In quantum information processing, information is encoded in individual quanta. The light provides natural resource for encoding information into state of light due to its weak enviromental interaction. To improve the density of the coded information we use hyper-encoding technique where two or more quantum bits are encoded into single photon. Coding information into single photon is dependant on how many degrees of freedom it has. Theoretically speaking it can be infinite since the Hilberts space can be infinite but technically speaking there are just few options how to code a quantum bit. Most common are spatial [1], polarisation [2] and time encoding.

In my thesis you will be introduced to experimental realization of a convertor betweeen polarization and spatial coding. We characterize it using full tomography measurement and linear inversion method [3]. In the next part we extent this idea to build tunable polarization filter using calcite beam displacers and mirrors. Although the mirrors are specially designed to minimalize its phase disturbance we found out that phase disturbance is non negligible. We prepared different polarization filthers and characterize them using full tomography measurements and maximum likelihood method [4]. We use the core of the setup to realize spatial and polarization encoding simontaneusly.

Chapter 1

Theory

1.1 Polarization

Consider a monochromatic wave of angular frequency ω traveling in the z direction with velocity v. The electric field lies in x-y plane and is described by

$$\vec{\mathrm{E}}(\mathrm{z},\mathrm{t}) = \mathrm{Re}\left\{\vec{\mathrm{A}}\exp\left[\mathrm{i}\left(\omega t - \frac{z}{v}\right)\right]\right\}, \tag{1}$$

where the complex envelope

$$\vec{\mathrm{A}} = A_x\,\vec{e}_x + A_y\,\vec{e}_y\,, \tag{2}$$

is a vector with components A_x and A_y. To describe polarization of this wave we trace the endpoint of the vector E at each position z as a function of time.

Substituting (2) into (1) and expanding to Cartesian basis we obtain parametric equations of polarization elipse

$$\begin{aligned}\vec{\mathrm{E}}_{\mathrm{x}}(\mathrm{z},\mathrm{t}) &= |A_x|\cos\left[\left(\omega t - \frac{z}{v} + \arg(A_x)\right)\right]\\ \vec{\mathrm{E}}_{\mathrm{y}}(\mathrm{z},\mathrm{t}) &= |A_y|\cos\left[\left(\omega t - \frac{z}{v} + \arg(A_y)\right)\right]\end{aligned}. \tag{3}$$

We can rewrite the parametric equations (3) into the implicit form of ellipse equation

$$\left(\frac{E_x}{A_x}\right)^2 + \left(\frac{E_y}{A_y}\right)^2 - 2\frac{E_x}{A_x}\frac{E_y}{A_y}\cos(\delta) = \sin^2(\delta)\,, \tag{4}$$

where δ is phase difference.

1.2 Jones Formalism

Jones formalism is used to describe light in a pure polarization state. Jones vector has the form of

$$\vec{J} = \begin{pmatrix} A_x \\ A_y \end{pmatrix}. \tag{5}$$

Arbitrary pure polarization state may be described using polarization ellipse and its parameters ellipticity χ and orientation to positive x-semiaxis ψ. Jones vector can be rewritten in notion of elliptical parameters

$$\vec{J}(\chi,\psi)=\begin{bmatrix}\cos(\psi)\cos(\chi)-i\sin(\psi)\sin(\chi)\\ \sin(\psi)\cos(\chi)+i\cos(\psi)\sin(\chi)\end{bmatrix}. \tag{6}$$

Parameters of the polarization ellipse are obtained from relation (5) and (6)

$$\begin{aligned}\psi &= \frac{1}{2}\arctan\left[\frac{2\sqrt{A_x A_x^* A_y A_y^*}}{A_x A_x^* - A_y A_y^*}\cos\left(\arg\left(\frac{A_y}{A_x}\right)\right)\right],\\ \chi &= \frac{1}{2}\arctan\left[A_x^2 + A_y^2\right]\end{aligned} \tag{7}$$

Every environment that can change polarization state, can be described by transformation matrix

$$T=\begin{bmatrix}a_{11} & a_{12}\\ a_{21} & a_{22}\end{bmatrix}, \tag{8}$$

where $a_{ij} \in C$ for $i,j = 1,2$.

We describe the transformation matrix of multiple environments $1,2,\ldots n$ described by matrices $T_1, T_2, \ldots, T_n$ as

$$T = T_n \ldots T_2 \cdot T_1. \tag{9}$$

For example we show the matrices for the most frequently used optical devices. The polarizer rotated by angle α is described by matrix

$$\begin{aligned}POL(\alpha) &= \begin{bmatrix}\cos(\alpha) & -\sin(\alpha)\\ \sin(\alpha) & \cos(\alpha)\end{bmatrix}\cdot\begin{bmatrix}1 & 0\\ 0 & 0\end{bmatrix}\cdot\begin{bmatrix}\cos(\alpha) & \sin(\alpha)\\ -\sin(\alpha) & \cos(\alpha)\end{bmatrix} =\\ &\begin{bmatrix}\cos^2(\alpha) & \cos(\alpha)\sin(\alpha)\\ \cos(\alpha)\sin(\alpha) & \sin^2(\alpha)\end{bmatrix}.\end{aligned} \tag{10}$$

The retarder plate which causes phase difference Γ rotated by angle α is described by matrix of form

$$RET(\alpha)(\Gamma)=\begin{bmatrix}\cos(\alpha) & -\sin(\alpha)\\ \sin(\alpha) & \cos(\alpha)\end{bmatrix}\cdot\begin{bmatrix}1 & 0\\ 0 & e^{-i\Gamma}\end{bmatrix}\cdot\begin{bmatrix}\cos(\alpha) & \sin(\alpha)\\ -\sin(\alpha) & \cos(\alpha)\end{bmatrix}. \tag{11}$$

Where in case $\Gamma=\pi$, we have matrix for half wave plate

$$HWP(\alpha)=\begin{bmatrix}\cos(2\alpha) & \sin(2\alpha)\\ \sin(2\alpha) & -\cos(2\alpha)\end{bmatrix}. \tag{12}$$

If $\Gamma=\pi/2$ we have matrix for quarter wave plate

$$QWP(\alpha)=\begin{bmatrix}\cos^2(\alpha)-i\sin^2(\alpha) & (1+i)\cos(\alpha)\sin(\alpha)\\ (1+i)\cos(\alpha)\sin(\alpha) & -i\cos^2(\alpha)+\sin^2(\alpha)\end{bmatrix}. \tag{13}$$

1.3 Stokes formalism

Stokes formalism is used to describe partially polarized states of light. Every state can be mapped on Bloch sphere. We define the state with vector of lenght P which corresponds to degree of polarization. If $P < 1$ the light is not in pure state, if $P = 1$ the light is in completely pure polarization state and it is mapped on the surface of the Bloch's sphere. The longitude of the point is 2ψ and the latitude is 2χ, where ψ and χ are elliptical parameters of polarized part of light. We see that these elliptical parameters describe pure part of state. Let x, y, z be Cartesian coordinates of a point on the sphere. The Stokes vector consists of parameters:

$$\vec{S}=\begin{bmatrix}S_0\\ S_1\\ S_2\\ S_3\end{bmatrix}=\begin{bmatrix}\sqrt{x^2+y^2+z^2}\\ x\\ y\\ z\end{bmatrix}=\begin{bmatrix}P\\ P\cdot\cos(2\psi)\cos(2\chi)\\ P\cdot\sin(2\psi)\cos(2\chi)\\ P\cdot\sin(2\chi)\end{bmatrix}. \tag{14}$$

We define degree of polarization as

$$P=\sqrt{{S_1}^2+{S_2}^2+{S_3}^2}. \tag{15}$$

Known ellipse parameters ψ, χ could be used as a transition from Stokes to Jones formalism using (6) and from Jones to Stokes using (7) and (14). Due to occurrence of *arctan* function we are facing $\pi/4$-periodicity problem, so we have to be careful using these relations. Relation between Jones and Stokes formalism is shown in table *1*.

Table 1: Table of main states in Jones and Stokes formalism.

State name	***State ket***	***Jones Formalism***	***Stokes Formalism***	***Semiaxis position ψ***	***Ellipticity χ***
Horizontal	$\|H\rangle$	$\begin{bmatrix}1\\0\end{bmatrix}$	$\begin{bmatrix}1\\1\\0\\0\end{bmatrix}$	0	0
Vertical	$\|V\rangle$	$\begin{bmatrix}0\\1\end{bmatrix}$	$\begin{bmatrix}1\\-1\\0\\0\end{bmatrix}$	90	0
Diagonal	$\|D\rangle$	$\frac{1}{\sqrt{2}}\begin{bmatrix}1\\1\end{bmatrix}$	$\begin{bmatrix}1\\0\\1\\0\end{bmatrix}$	45	0
Antidiagonal	$\|A\rangle$	$\frac{1}{\sqrt{2}}\begin{bmatrix}1\\-1\end{bmatrix}$	$\begin{bmatrix}1\\0\\-1\\0\end{bmatrix}$	-45	0
Right Circular	$\|R\rangle$	$\frac{1}{\sqrt{2}}\begin{bmatrix}1\\i\end{bmatrix}$	$\begin{bmatrix}1\\0\\0\\1\end{bmatrix}$	-	45
Left Circular	$\|L\rangle$	$\frac{1}{\sqrt{2}}\begin{bmatrix}1\\-i\end{bmatrix}$	$\begin{bmatrix}1\\0\\0\\-1\end{bmatrix}$	-	-45

1.4 Interference of two partially coherent waves

Let say we have a partially coherent wave *E(z,t)* described by equation (1) where the value of amplitude *A(z,t)* varies with time *t* and position *z*. If *E(z,t)* is added to its own replica delayed by the time τ we can define the interference pattern as

$$I = 2I_0\left[1+\left|g(\tau)\right|\cos\left(\varphi(\tau)\right)\right], \tag{16}$$

where $\varphi(\tau)$=argg$(\tau)\}$. So the ability of the wave to interfere with is time delayed replica is depended by its complex degree of temporal coherence. We can define the strength of the interference by the visibility *V*

$$V = \frac{I_{\max} - I_{\min}}{I_{\max} + I_{\min}}, \tag{17}$$

where I_{max} and I_{min} are maximum and minimum intensity as τ changes its value. We can see an relation between intensity *I* and time delay τ called interferogram on the figure 1.

Figure 1: Normalized intensity $I/2I_0$ as a function of time delay τ [1].

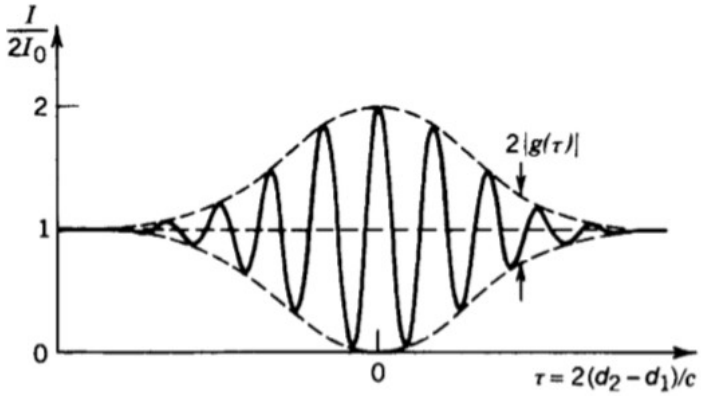

We can see from the figure 1 that when $\tau=0$ (there is no optical path difference) we find the maximum intensity and the strongest visibility.

1.5 One qubit tomography and polarization state reconstruction

Lets suppose we have an unknown polarization state which is represented by its density matrix. In order to reconstruct its density matrix we measure intensities in particular projections. We use projections to |H>, |D>, |R> basis. From measured intensities we can calculate propabilities of finding the state in the given projection:

$$\left\langle H\left|\hat{\rho}\right|H\right\rangle = \rho_H = \frac{I_H}{I_H + I_V},$$
$$\left\langle D\left|\hat{\rho}\right|D\right\rangle = \rho_D = \frac{I_D}{I_D + I_A}, \tag{18}$$
$$\left\langle R\left|\hat{\rho}\right|R\right\rangle = \rho_R = \frac{I_R}{I_R + I_L},$$

where $\hat{\rho}$ is a density matrix. From equation (18) we can obtain Stokes parameters define

$$S_1 = 2\rho_H - 1, \tag{19}$$
$$S_2 = 2\rho_D - 1, \tag{20}$$
$$S_3 = 2\rho_R - 1, \tag{21}$$
$$S_0 = \sqrt{(S_1^2 + S_2^2 + S_3^2)}\ . \tag{22}$$

From obtained Stokes vectors we are able to reconstruct density matrix in a following way

$$\hat{\rho} = \frac{1}{2}\sum_{i=0}^{3} S_i \hat{\sigma}_i \tag{23}$$

where S_i are Stoke's vectors and $\hat{\sigma}_i$ are Paulie matrices. Purity of state is defined as

$$P = Tr(\rho^2)\ . \tag{24}$$

Please note that equation (24) and equation (22) are identical. Another property we are going to deal with is fidelity. Fidely defines overlap between two density matrices. Fidelity of two states is defined as

$$F(\rho, \sigma) = Tr\{[(\sigma)^{1/2}\rho(\sigma)^{1/2}]^{1/2}\}^2\ . \tag{25}$$

1.6 Maximum likelihood reconstruction method

Another reconstruction method is maximum likelihood method. Let us assume we have finite number *N* of identical samples of the physical system, each in the same but unknown quantum state described by density operator ρ. Our task is to reconstruct the unknown quantum state ρ from the measurements performed on them. We consider the positive operator-valued measure (POVM) Π_l that yields propabilities p_l of individual outcomes,

$$p_l = Tr[\rho\,\Pi_l],\ p_l \geq 0,\ \sum_l p_l = 1\ . \tag{26}$$

If POVM is tomographically complete, it is possible to determine the true state ρ directly by inverting linear relations (27) between propabilities p_l and the elements of density matrix ρ. However, there is no way to find out the exact probabilities since only finite

number N of samples of the system can be investigated. In case of N_l occurrences of the outcome Π_l, the relative detection frequencies $f_l = N_l / N$ represent the only data that could be used for reconstruction of our unknown true state. The maximum likelihood approach to this reconstruction problem consists in finding a density operator ρ_{est} that generates, probabilities (27) that are as close to the observed frequencies f_l as possible

$$\rho_{est} = arg \max_{\rho} L[f_l, p_l(\rho)], \tag{27}$$

$$L[f_l, p_l(\rho)] = \sum_l f_l \ln p_l. \tag{28}$$

It can be shown that the reconstruction procedure can be interpreted as a generalized POVM measurement if the log-likelihood measure (28) is used.

Analytical approach to the problem of maximization (27) of the log-likelihood functional (28) involves a formulation of nonlinear extremal operator equation for the density matrix that maximizes the log-likelihood functional,

$$\rho = \mu^{-1} R \rho, R = \sum_l \frac{f_l}{p_l} \Pi_l, \tag{29}$$

where μ is Lagrange multiplier in form

$$\mu = Tr[R \rho] = \sum_l f_l = 1. \tag{30}$$

Advantage of the equation (29) is that it might have an iterative solution. Equation (29) and its hermitian conjugate leads to the symmetric extremal equations in the manifestly positive semidefinite form

$$\rho = \mu^{-2} R \rho R, \mu = \left(Tr[R \rho R] \right)^{1/2}. \tag{31}$$

Iterations given by

$$\rho^{(n+1)} = \mu^{(n)-2} R^{(n)} \rho^{(n)} R^{(n)} \tag{32}$$

preserve the positive semidefiniteness and trace normalization of the density operator ρ.

1.7 Reconstruction of process matrix (completely positive CP map)

The linear completely positive (CP) map describes the transformation of physical system from quantum state ρ_{in} to quantum state ρ_{out}. The mathematical formulation of CP maps relies on the isomorphism between linear CP maps M_s from operators on the Hilbert space H to operators on Hilbert space K and positive semidefinite operators S on Hilbert space $H \otimes K$

$$\rho_{out} = M_S[\rho_{in}] = Tr_H[S\,\rho_{in}^T \otimes 1_K], \tag{33}$$

where T is transposition and 1_K is identity operator on K space. The deterministic quantum transformations preserve the trace of the transformed operators. This must hold for any input state ρ_{in}, the operator S must satisfy the condition

$$Tr_K[S] = 1_H, \tag{34}$$

where 1_H is identity operator on H space.

Let ρ_m denote various input states from space H, which are used for probing of the quantum process. Measurements described by POVMs Π_{ml} are carried out on each corresponding output state from space K. Let f_{ml} denotes the relative frequency of the corresponding detection of POVM element. The estimated operator S should maximize the constrained log-likelihood functional

$$L_c[f_{ml}, p_{ml}(S)] = \sum_{m,l} f_{ml} \ln p_{ml} - Tr[\Lambda S] \tag{35}$$

$$p_{ml} = Tr[S\,\rho_m^T \otimes \Pi_{ml}], \tag{36}$$

where $\Lambda = \lambda \otimes 1_K$ and λ is the matrix of Lagrange multipliers that account for the trace-preservation condition (34). The extremal equations for S can be obtained by varying functional (35) with respect to S,

$$L_c[f_{ml}, p_{ml}(S+\delta S)] - L_c[f_{ml}, p_{ml}(S)] = 0, \tag{37}$$

$$Tr\left[\left(\sum_{m,l} \frac{f_{ml}}{p_{ml}} \rho_m^T \otimes \Pi_{ml} - \Lambda\right)\delta S\right] = 0, \tag{38}$$

for all δS, which leads to

$$S = \Lambda^{-1} K S,\ K = \sum_{m,l} \frac{f_{ml}}{p_{ml}} \rho_m^T \otimes \Pi_{ml}. \tag{39}$$

We arrive at symmetrical expression suitable for iterations,

$$S = \Lambda^{-1} K S K \Lambda^{-1}. \tag{40}$$

The Lagrange multiplier λ must be determined from constraint (34)

$$\lambda = (Tr_K[KSK])^{1/2}. \tag{41}$$

The operator Λ is positive definite. Equations (40) and (41) may be solved numerically by iterations starting from some unbiased map. Equation (40) preserves the positive

semidefiniteness of S and constraint (34) is satisfied in each step. We can define process fidelity by

$$F_{\chi}=\frac{Tr[SS_{id}]}{Tr[S]Tr[S_{id}]}, \tag{42}$$

where S_{id} is theoretical process matrix. Theoretical process matrix is defined as

$$S_{id}=\frac{(1\otimes N)\Phi(1\otimes N^{+\cdot})}{Tr[(1\otimes N)\Phi(1\otimes N^{+\cdot})]}, \tag{43}$$

where N is general transformation, N^{+} is its hermitian conjugate, Φ= |Φ><Φ|=|HH>+|VV> is maximally entagled Bell state.

Chapter 2

Experiment

2.1 Converter between polarization and spatial modes

Our first goal is to construct converter between polarization and spatial modes. This is done by building *28 cm* long Mach-Zehnder interferometer using calcite beam displacers and reaching the highest possible visibility. Experimental setup of our converter is shown in figure 2.

Figure 2: Converter between polarization and spatial modes.

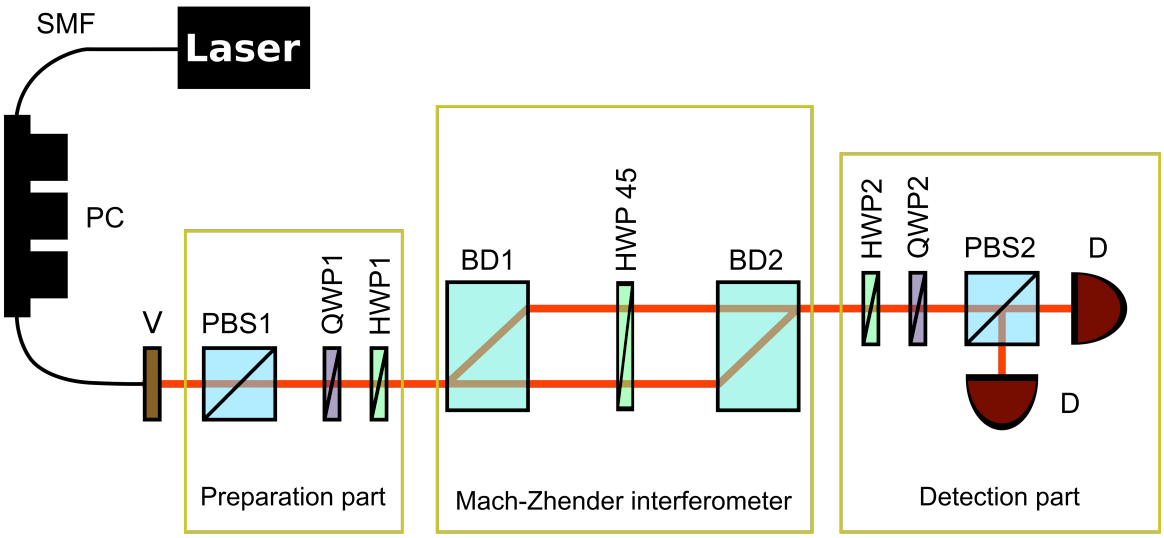

I used temperature controller THORLABS TED200C which was set on *12 kΩ*, THORLABS LED200C laser diode controller with operating current set on *100 mA* and LED diode which produces laser beam with center wavelength of *805 nm* that is coupled to NUFERN single mode optical fibre (SMF). Using polarization controller (PC) I was able to adjust the laser beam to be maximally horizontally polarized. Laser beam then leaves the collimator and interacts with EKSMA *99.9* polarization beam splitter which reflects vertically polarized light and transmits horizontally polarized light. For detection of our intensities we used THORLABS power meter set to measure in Volts. I adjusted the height of the laser beam to be set up on *90 mm.* Before any optical component was adjusted I checked the back reflection. I also tried to aim the laser beam to the center of every optical component so I could achieve lowest measurement errors.

I put first calcite beam displacers (BD1) behind the PBS1. Thanks to its birefringence, vertically polarized light goes through the calcite without changing its direction while horizontally would change. Our calcite is *10 mm* high, *10 mm* wide, *40 mm* long and since it acts like a beam displacer the distance between vertical and horizontal output is *4 mm*. I had to set up the reference plane of the calcite accordingly to output plane formed by vertical and horizontal light so it would be approximately parallel to optical table. To prevent cutting off the output of horizontal polarized light, I aimed the laser to be *1-2 mm* next to the center of BD1. Next step was calibration of waveplates which is crucial for the preparation and detection of polarization state. I calibrated the waveplates between

PBS1 and BD1. More details of waveplate calibration is described in appendix 1. After calibration of waveplates I put QWP1 and HWP1 in front of BD1.

In order to achieve interference at the edge of second BD2 I put half waveplate HWP 45 behind BD1. It was set up to 45 degrees. This changes horizontal polarization into vertical polarization and vise versa. Behind HWP 45 I put second calcite BD2 and rotated the BD2 along its optical axis so the *x-y* axes of the second calcite had been set up identically to the *x-y* axes of the first calcite. Behind the BD2 I adjusted the detection part which consists of HWP2, QWP2 and PBS2.

In order to measure visibility I had to set diagonally polarized light in the preparation and detection part of the setup. Angles needed for preparation and detection of the polarization state are described in Appendix 2. By changing the horizontal tilt of BD2 I changed the path difference in the Mach-Zehnder (MZ) interferometer. When I reached the minimum optical path difference I reached the highest visibility possible. By measuring the output intensity at both output ports behind PBS2 I was able to calculate the visibility of the interference. Maximum reached visibility was *0,950*. Reason why we could not reach higher visibility is because the spatial overlap of the both interfering waves is not perfect. To solve this problem we can couple the output signal into single mode optical fibre.

Next step was to characterize this device by state and process tomography. In preparation part I prepared six polarization states - horizontal |H>, vertical |V>, diagonal |D>, antidiagonal |A>, right circular |R> and left circular |L> polarazation. For every polarization state I had to set up the detection part for six polarization projections |H>, |V>, |D>, |A>, |R>, |L> respectively. I measured 6 intensities for every prepared polarization state and results are shown in table 2.

Table 2: Measured intensities for six polarizations states.

Projection → Basis ↓	$I_{\|H\rangle}$ [mV]	$I_{\|V\rangle}$ [mV]	$I_{\|D\rangle}$ [mV]	$I_{\|A\rangle}$ [mV]	$I_{\|R\rangle}$ [mV]	$I_{\|L\rangle}$ [mV]
$\|H\rangle$	0,000	0,007	0,209	0,211	0,207	0,206
$\|V\rangle$	0,000	0,000	0,207	0,212	0,215	0,205
$\|D\rangle$	0,205	0,215	0,418	0,015	0,210	0,221
$\|A\rangle$	0,205	0,208	0,010	0,410	0,221	0,199
$\|R\rangle$	0,224	0,232	0,238	0,234	0,415	0,008
$\|L\rangle$	0,234	0,228	0,232	0,236	0,010	0,415

As expected I detected the highest intensity in such polarization projection/analyses in which we prepare the state in. From the measured intensities I was able to reconstruct the polarization state and its Stokes vectors. The visualisation of Stokes vectors on Bloch sphere are shown on figure 3. In ideal case Stokes vectors would appear exactly on individual axes corresponding their polarization state. We can see that they are slightly off. By solving equations (14) we can find the longitudinal 2ψ and latitudinal 2χ angles which says how many degrees they are off the axes. I also calculated purity P using equation (15) and determined whether the polarization state is mixed or pure. Purity P and other parameters are calculated in table 3. Please note that purity P and other parameters are calculated from raw experimental data which contains detector noise. The detector noise is considered to be the dark current of the detector and incident light from the room. I measured it when I blocked laser beam and its value is *0,0062 mV*. I also analysed data

without detector noise. I took the value of detector noise and subtracted it from the measured data in table 2. I received new set of data, from which I calculated purity *P'* and other parameters which are shown in table 4. We can see that by subtracting the value of noise from the measured data the purity of the states increases.

Table 3: Calculated purity P, Stokes parameters S of reconstructed polarization state, longitudinal 2ψ and latitudinal 2χ angles.

Stokes parameter → / Basis ↓	*P*	S_1	S_2	S_3	*2ψ (degrees)*	*2χ (degrees)*
$\|H\rangle$	0,976	0,976	0,002	0	0,14	0
$\|V\rangle$	0,971	-0,972	0,023	0	1,41	0
$\|D\rangle$	0,931	-0,024	0,023	0,931	-90,0	87,95
$\|A\rangle$	0,954	-0,007	0,048	-0,952	88,33	-87,11
$\|R\rangle$	0,962	-0,018	0,962	0,008	88,96	0,51
$\|L\rangle$	0,953	0,012	-0,953	-0,009	-89,22	-0,51

Table 4: Calculated purity P', Stokes parameters S' of reconstructed polarization state, longitudinal 2ψ and latitudinal 2χ angles.

Stokes parameter → / Basis ↓	*P'*	S_1'	S_2'	S_3'	*2ψ´ (degrees)*	*2χ´ (degrees)*
$\|H\rangle$	0,995	0,995	0,003	0	0,14	0
$\|V\rangle$	1,000	-1,000	0,025	0	1,40	0
$\|D\rangle$	0,961	-0,053	-0,024	0,958	-90,0	86,51
$\|A\rangle$	0,982	-0,007	0,049	-0,982	88,32	-87,11
$\|R\rangle$	0,991	-0,018	0,991	0,009	88,96	0,50
$\|L\rangle$	0,982	0,013	-0,982	-0,009	-89,22	-0,51

Figure 3: We can see the visual interpretation of Stokes vectors on Bloch's sphere. Where axes S1, S2, S3 interprete the individual dimensions of Hilbert's space. S1 represents $|H\rangle$, $|V\rangle$ polarization, S3 represents $|D\rangle$, $|A\rangle$ polarization and S2 represents $|R\rangle$, $|L\rangle$ polarization. First picture represents reconstructed $|H\rangle$ state, second $|V\rangle$, third $|D\rangle$, fourth $|A\rangle$, fifth $|R\rangle$, sixth $|L\rangle$.

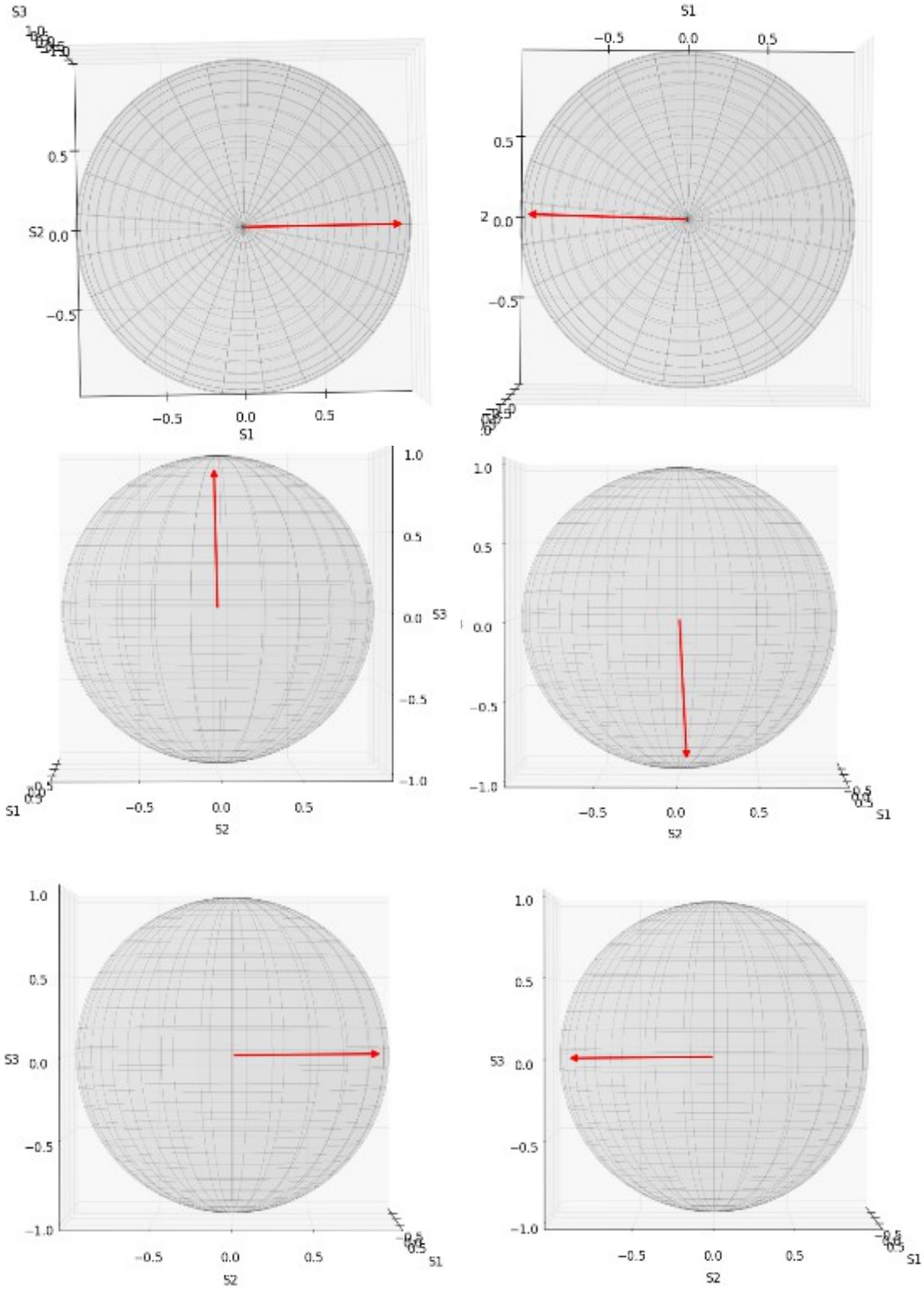

I interpreted polarization state with its density matrix calculated from data without considering detectors noise and reconstructed our density matrices by using equation (20). From the density matrices I was able to calculate fidelity according to equation (22). I calculated fidelity F between reconstructed density matrix from data and theoretical density matrix defined on input. If fidelity is equal to one the reconstructed state is identical to the input state. This means our operation is described by identity. Reconstructed density matrices with calculated purities and fidelities are shown in figure 4. We can see that in all cases fidelity are very close to one.

Figure 4: Reconstructed density matrices with linear inversion method.

Real part of |H> polarization state.

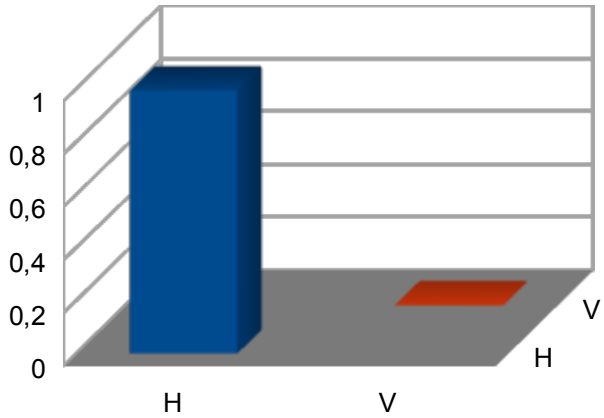

P′ = 0,995 *F = 0,998*

Real part of |V> polarization state.

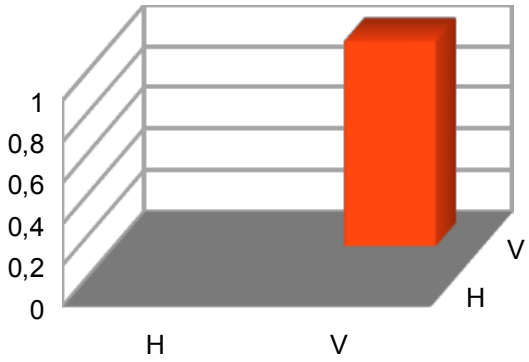

P′ = 1,0 *F =1,0*

Real part of |D> polarization state.

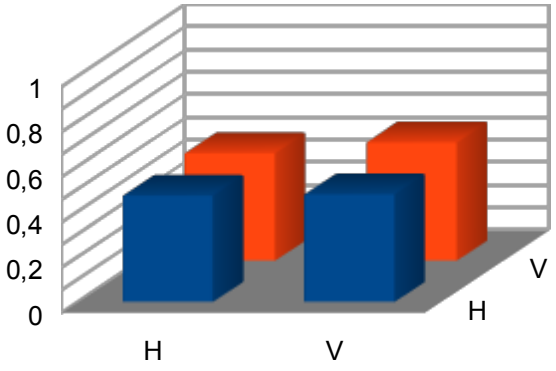

P′ = 0,961 *F = 0,979*

Real part of |A> polarization state.

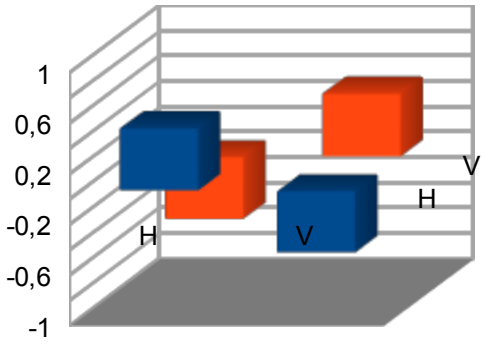

P′ = 0,982 *F = 0,991*

Real part of |R> polarization state. *Imaginary part of |R> polarization state.*

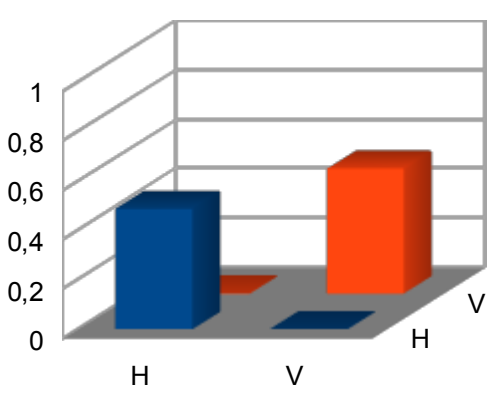

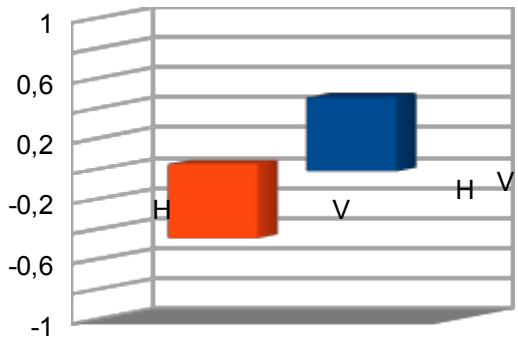

$P' = 0{,}991$ $F = 0{,}996$

Real part of |L> polarization state. *Imaginary part of |L> polarization state.*

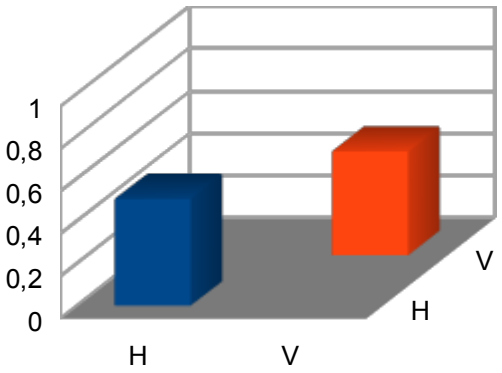

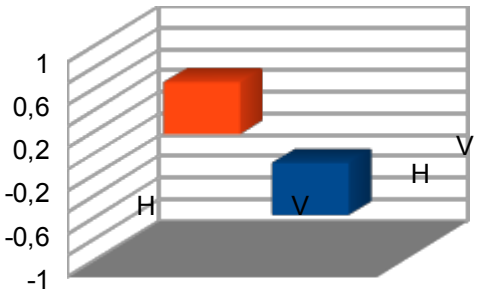

$P' = 0{,}982$ $F = 0{,}991$

From the complete tomografic results I was able to reconstruct the experimental process matrix. Experimental process matrix is usefull for characterisation of our device. It helps us to calculate the output density matrix from input density matrix without any further measurement, see equation (33). Reconstructed experimental process matrix is shown in figure 5. Theoretical process matrix is shown in figure 6. From theoretical and experimental process matrix I calculated process fidelity F_χ (37) which describes the overlap beetween experimentaly measured and theoreticaly calculated process matrix. Process fidelity is very close to *1* which means that our mode convertor works as it was designed.

Figure 5: Experimental polarization state process matrix.

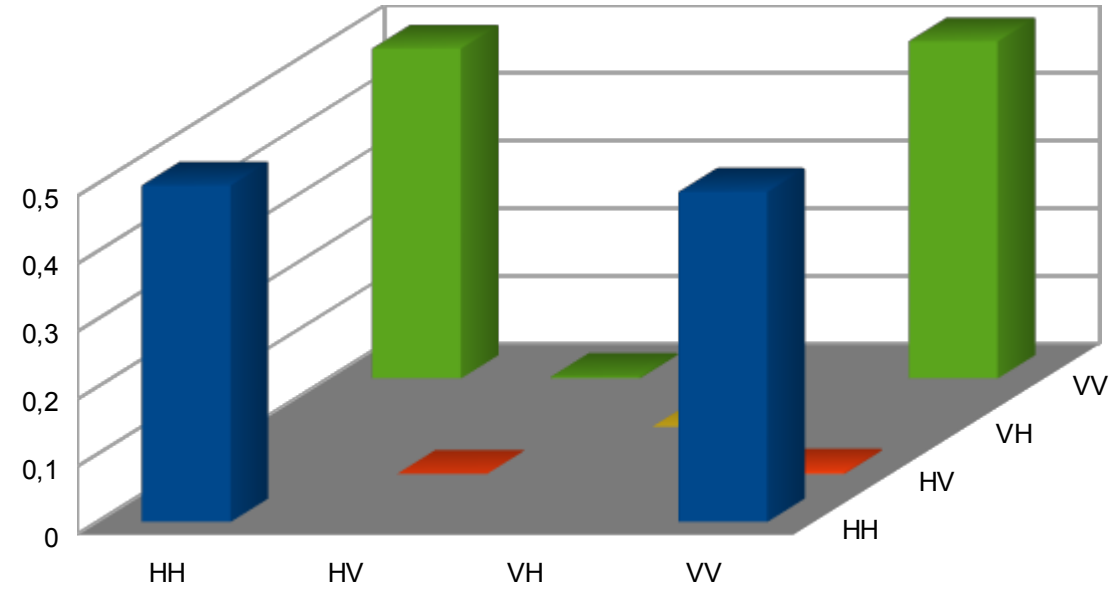

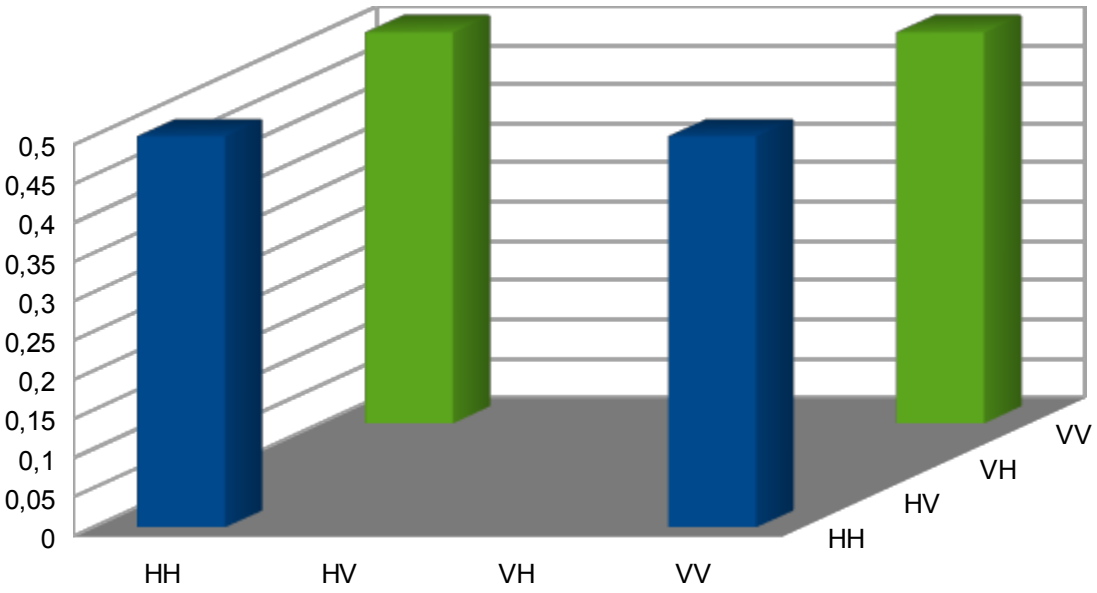

Figure 6: Theoretical polarization process matrix.

$$F_{\chi} = 0{,}988$$

2.2 Preparation of MZ interferometer for hyper-encoding

In last section we were dealing with the encoding information into spatial mode of the light. Since our final goal is to encode information to spatial and polarization degree of freedom of the light we had to reorganize the experimental setup. To get more space in the Mach-Zehnder interferometer we added two FEMTOLASSER mirrors, see fig 7. This increased the length of the Mach-Zehnder interferometer from *28 cm* to *72 cm*. Mirrors generaly change the polarization state of the reflected light but ours were designed to change it minimaly. The angle of incidence for both mirrors was approximately *45* degrees.

Figure 7: Converter between polarization and spatial coding with mirrors.

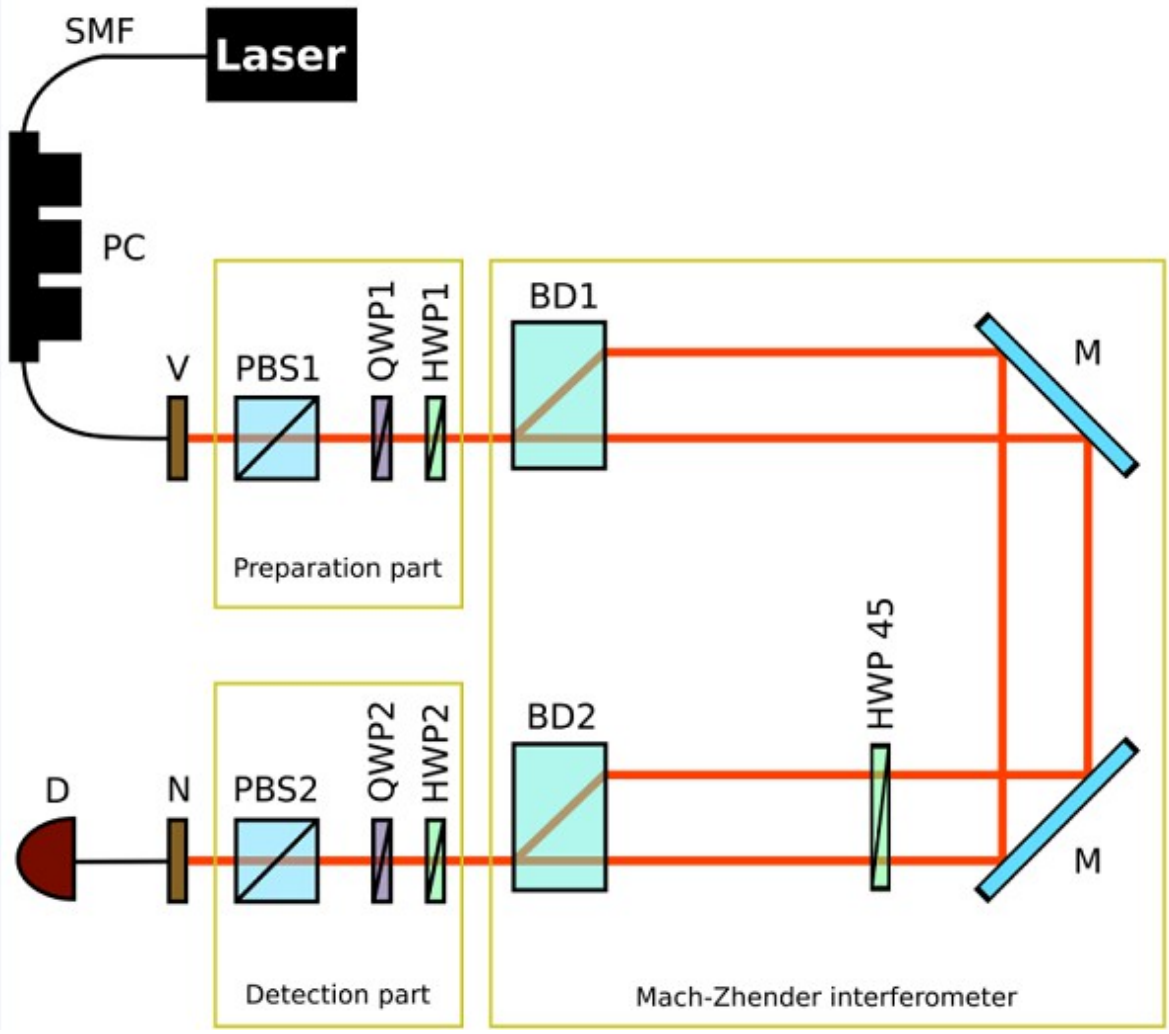

Building the experiment was almost identical to previous case described in section *2.1*. The only difference was that this time I used PIN photodiode detector which was set to measure intensities in ampers *A*. I set up the preparation and detection part for diagonal polarization. By changing the horizontal position of BD2 I was searching for highest visibility. Obtained visibility was only *0,633*.

To compensate the phase of the MZ interferometer and to obtain higher visibility I added phase plates into experimental setup. First I added the one I tilted manually. I put one VOD phase plate to each trajectories of the interferometer. Initially, the incident beam was perpendicular to the plates plane. I tilted BD2 horizontally. I found the highest

visibility on its horizontal scale. Then I tilted one phase plate horizontally. By tilting the phase plate I also changed the optical path difference in the Mach-Zehnder interferometer. Repating this method the highest visibility I was able to find was V=*0,724*.

To locate highest visibility faster I used phase plates where one was fixed and second was automatically rotating using external electrical source. They were pieces of glass from the same phase plate so the width was the same for both. We set up the electrical voltage of the source on *5V*. In this case I was able to scan the horizontal scale of BD2 on osciloscope. By changing the horizontal position of BD2 the interference pattern was changing. The goal was to find the biggest difference between highest and lowest intensity on the interferogram (similar to the one on figure 1). In that way I was able to find maximum visibility V= *0,841*.

In comparison to previous experiment from section *2.1* the visibility had decreased about *0,1*. Since the time difference between experiments was long we suspect there can be something with the laser source. We suspected that the coherent length of the source could have changed. In order to eliminate this alternative I decided to change the laser source to one with narrower bandwidth. Narrow bandwitdh leads to longer coherence time and longer coherence length. With the new source I was unable to find higher visiblitiy as before. This means that our suggestion is not the main cause of the problem and I changed the new laser source back to original one.

Next step was to check the power difference in both separated laser beams behind BD1 after diagonal polarization preparation. So I blocked one beam behind BD1 and measured the power of the second beam with power meter and vice versa. I found out that there was a power difference between upper and lower path. By slightly rotating the first calcite I managed to change the power in each path to be *50%* of the full power. By rotating the second calcite I wanted to fix the *x-y* plane to be identical to the first calcite. Then I was searching for the highest visibility. The estimated visibility was V=*0,901*.

Because of the BD1 rotation we lost polarization frame reference and I decided to build the experiment from the beginning and recalibrate all optical components again. Moreover I decided to remove phase plates from the experimental setup. Once the experimental setup was finished I measured visibility of V=*0,945,* which is comparable to experiment in previous section.

Following the suggestion about spatial overlap from last section I decided to couple the optical signal into single mode fiber NUFERN HP780. I was able to reach V=*0,994* visibility and coupling efficiency of *0,849*. Now I was able to characterize this device by state tomography, see section 2.1. Measured intensities and estimated stokes parameters are shown in table 5 and 6, respectively.

Table 5: Measured intensities for different states and their projections.

Projection → / Basis ↓	$I_{\|H\rangle}$ [A]	$I_{\|V\rangle}$ [A]	$I_{\|D\rangle}$ [A]	$I_{\|A\rangle}$ [A]	$I_{\|R\rangle}$ [A]	$I_{\|L\rangle}$ [A]
$\|H\rangle$	0,841	0,0	0,441	0,436	0,428	0,376
$\|V\rangle$	0,0	0,828	0,423	0,418	0,429	0,366
$\|D\rangle$	0,418	0,417	0,758	0,091	0,151	0,654
$\|A\rangle$	0,416	0,412	0,071	0,768	0,648	0,168
$\|R\rangle$	0,414	0,421	0,128	0,683	0,732	0,121
$\|L\rangle$	0,432	0,349	0,711	0,131	0,114	0,733

Table 6: Stokes parameters and purity of polarization states.

Stokes parameter → / Basis ↓	S_1	S_2	S_3	P
$\|H\rangle$	0,994	0,059	0,0	0,000
$\|V\rangle$	-0,993	0,071	0,0	0,000
$\|D\rangle$	0,0	-0,632	0,791	0,988
$\|A\rangle$	0,011	0,589	-0,827	0,999
$\|R\rangle$	-0,011	0,719	-0,681	0,000
$\|L\rangle$	0,100	-0,742	0,686	0,988

From table 6 we can see that coupling laser beam to optical fiber lead to higher degree of polarization which is almost *1* in all cases this time. This means our states are located on the surface of Bloch's sphere where they are completely pure. Moreover the coupling signal into single mode fiber eliminated the detector noise.

If we compare data from table 4 and table 6 we can see that the Stokes vectors for $|H\rangle$ and $|V\rangle$ stayed the same but the Stokes vectors for $|D\rangle$, $|A\rangle$ and $|R\rangle$, $|L\rangle$ had changed. We conclude that a global phase change was present due to light reflection on mirrors. The visualisation of Stokes vectors on Bloch sphere are shown on figure 8. Solving the equation (14) and comparing table 7 to the table 4 we calculated that the Bloch's sphere had rotated *40* degrees counter clockwise in average. Calculated longitudinal *2ψ'* and latitudinal *2χ'* angles are shown in table *7*.

Table 7: Longitudinal 2ψ and latitudinal 2χ angles.

Angles → / Basis ↓	***2Ψ (degree)***	***2χ (degrees)***
$\|H\rangle$	3,21	0,13
$\|V\rangle$	3,76	0,21
$\|D\rangle$	-90	51,59
$\|A\rangle$	88,82	-54,91
$\|R\rangle$	89,04	42,82
$\|L\rangle$	-82,09	-43,41

Figure 8: We can see the visual interpretation of Stokes vectors on 3D Bloch's sphere using mirrors in experiment. Where axes S1, S2, S3 represent individual dimensions of Hilbert's space. S1 represents $|H\rangle$, $|V\rangle$ polarization, S3 represents $|D\rangle$, $|A\rangle$ polarization and S2 represents $|R\rangle$, $|L\rangle$ polarization. First picture represents reconstructed $|H\rangle$ state, second $|V\rangle$, third $|D\rangle$, fourth $|A\rangle$, fifth $|R\rangle$, sixth $|L\rangle$.

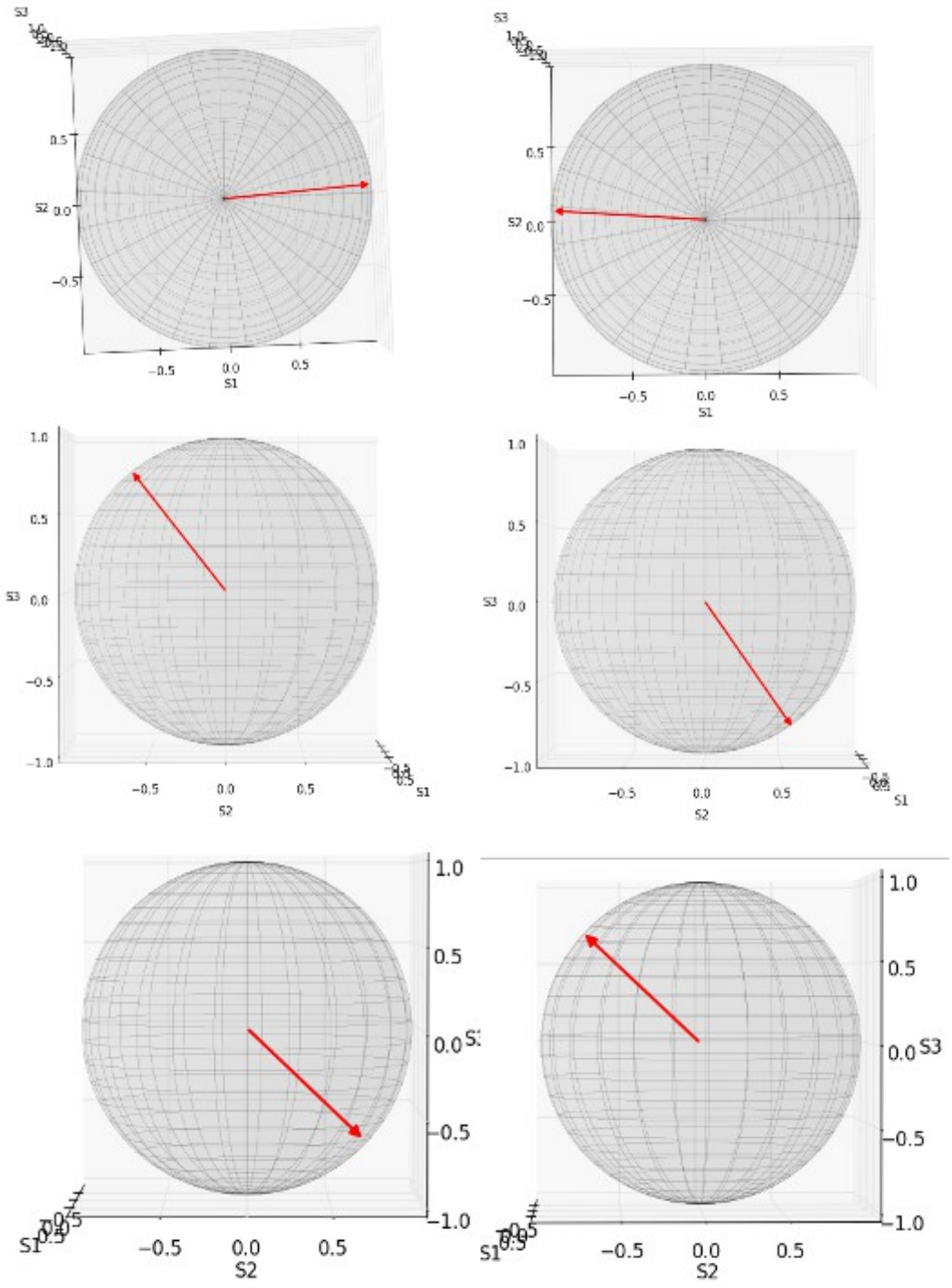

I described the polarization states with their density matrices. I reconstructed density matrices using maximum likelihood method and raw data from table 5. Reconstructed density matrices are shown in figure 9. From the density matrices I calculate the purity *P*. We can see that purities are very close to one.

I also calculated fidelity *F* of the states and we can see that fidelity is smaller than in previous experiment. This is because the Blochs equator had rotated counter-clockwise. Diagonally and antidiagonally states gained imaginary parts on their antidiagonals. Left circular and right circular polarization states gained real parts on their diagonals. This finding carried on also into estimation process fidelity. In comparison to the case without mirrors the process fidelity dropped about *0,1* to *0,886*. Reconstructed experimental polarization process matrix is shown on figure 10.

Figure 9: Reconstructed density matrix of the states using MAXLIK method.

Real part of |H> polarization state.

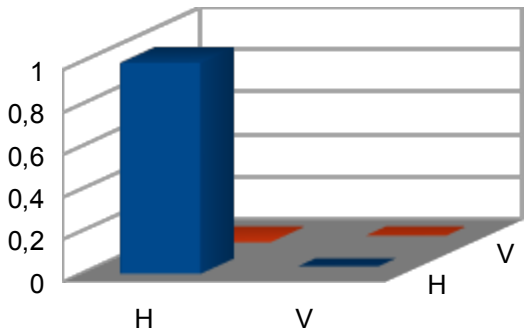

P=0,998 *F=0,999*

Real part of |V> polarization state.

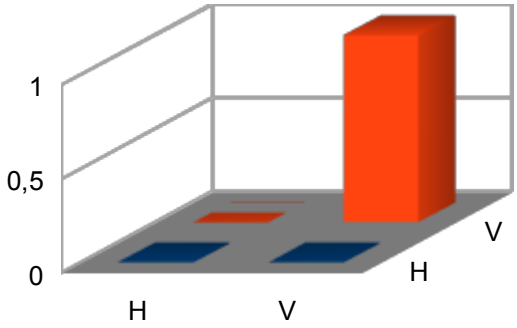

P=0,993 *F=0,996*

Real part of |D> polarization state

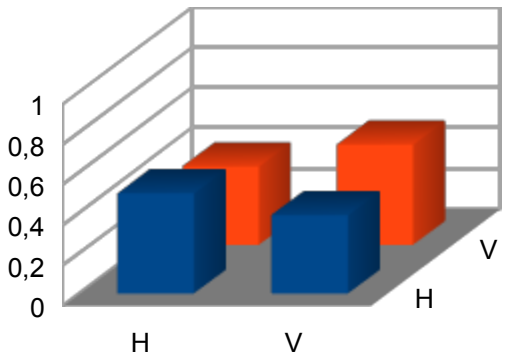

P=0,988

Imaginary part of |D> polarization state

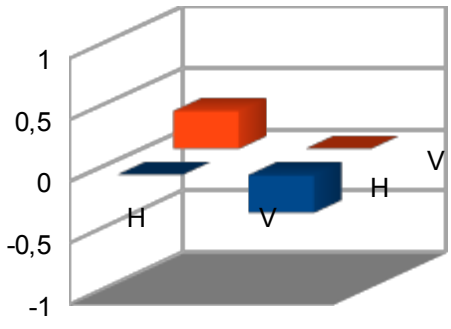

F=0,892

Real part of |A> polarization state.

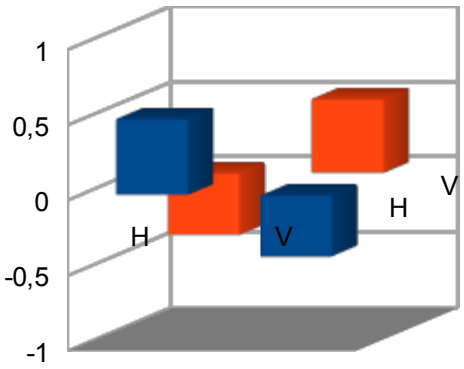

P'=0,999

Imaginary part of |A> polarization state.

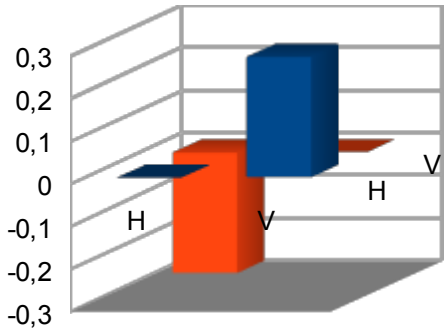

F=0,909

Real part of |R> polarization state.

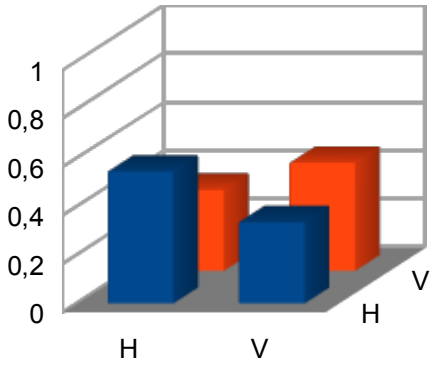

P=0,999

Imaginary part of |R> polarization state.

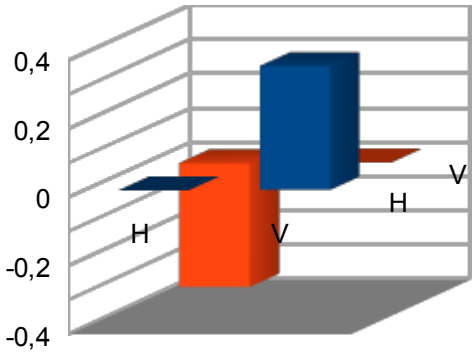

F=0,894

Real part of |L> polarization state.

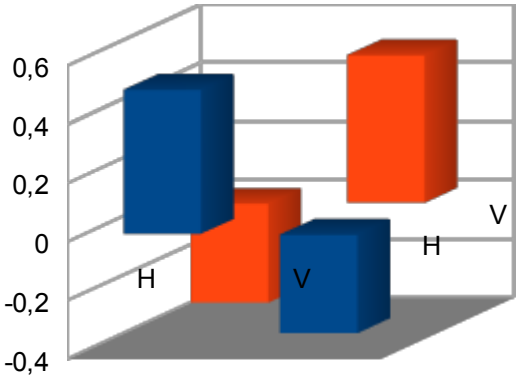

P=0,988

Imaginary part of |L> polarization state.

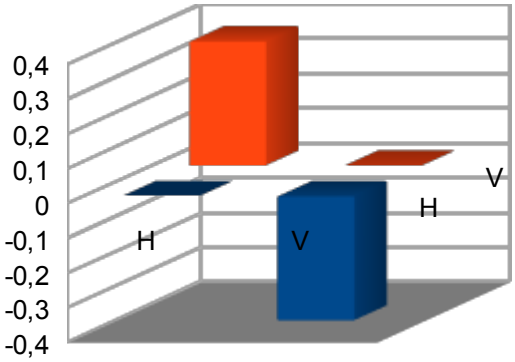

F=0,859

Figure 10: Reconstructed experimental process matrix with mirrors in the set up.

Real part of experimental process matrix.

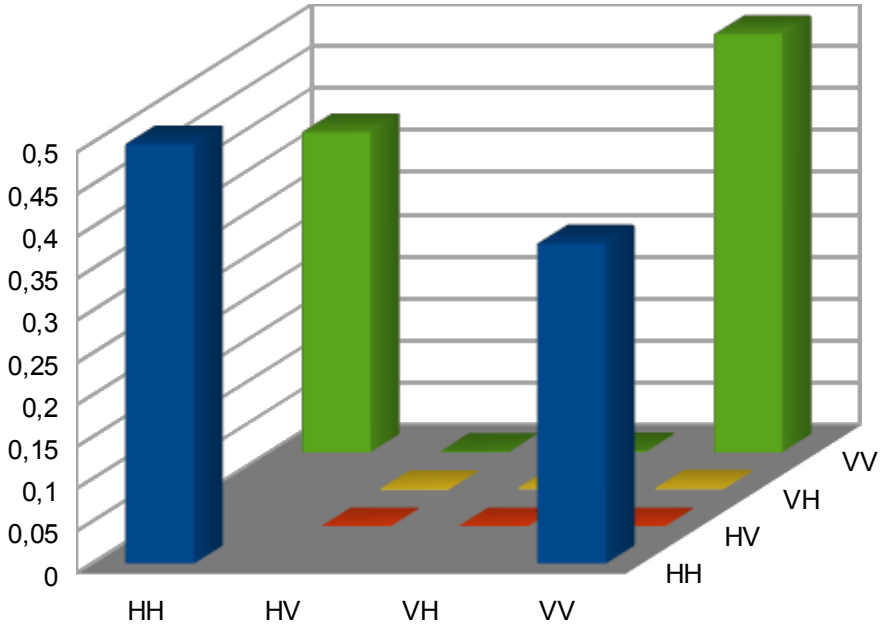

Imaginary part of experimental process matrix.

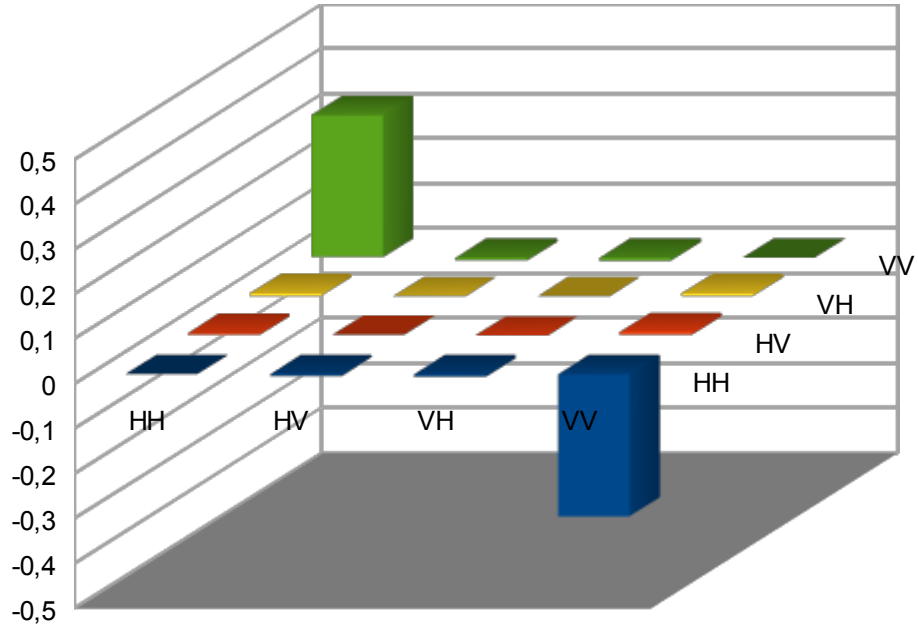

$F_{\chi} = 0{,}886$

Phase compensation

From previous results we came to a conclusion that Blochs equator had rotated counter-clockwise. This can be understood as a global phase shift. There are two ways to compensate the phase shift. One way is to do it experimentally by adding HWP and QWP into experimental setup. The second way is to find one unitary operation and compensate it numerically. In order to obtain highest possible fidelity we decided to find one suitable unitary operation. This was done by using phase matrix (see appendix 3) which I applied to all reconstructed matrices. The phase matrix rotates Blochs sphere *40* degrees clockwise. Calculated purities and fidelities before and after phase compensation are in table 8. I applied this unitary operation to experimental process and process fidelity raised from *0,886* to *0,995*. Compensated experimental process matrix is shown in figure 11.

Table 8: Calculated purities P, fidelities F before phase compensation and F' after phase compensation.

	P	***F***	***F'***
|H>	0,998	0,999	0,999
|V>	0,999	0,996	0,996
|D>	0,998	0,892	0,999
|A>	0,999	0,909	0,998
|R>	0,999	0,894	0,997
|L>	0,988	0,859	0,993

Figure 11: Compensated experimental process matrix.

Real part of experimental process matrix.

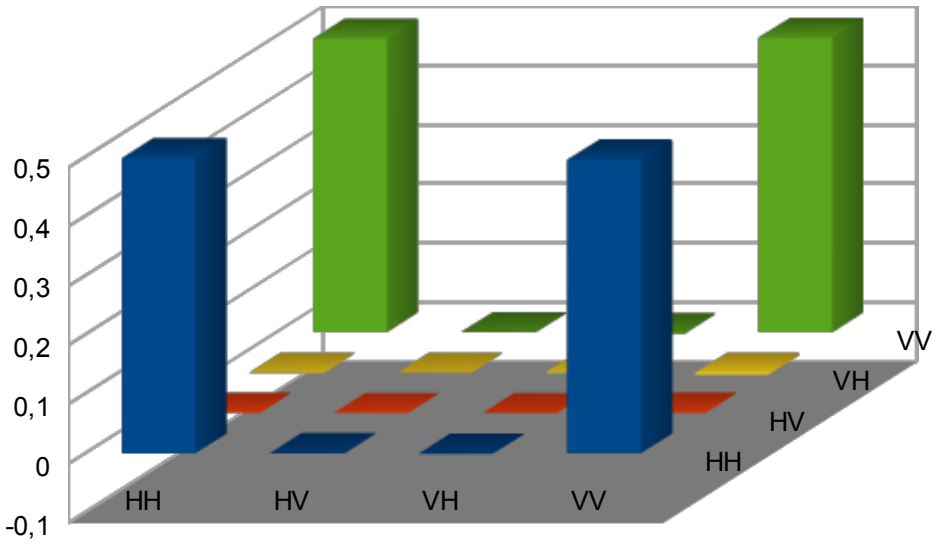

Imaginary part of experimental process matrix.

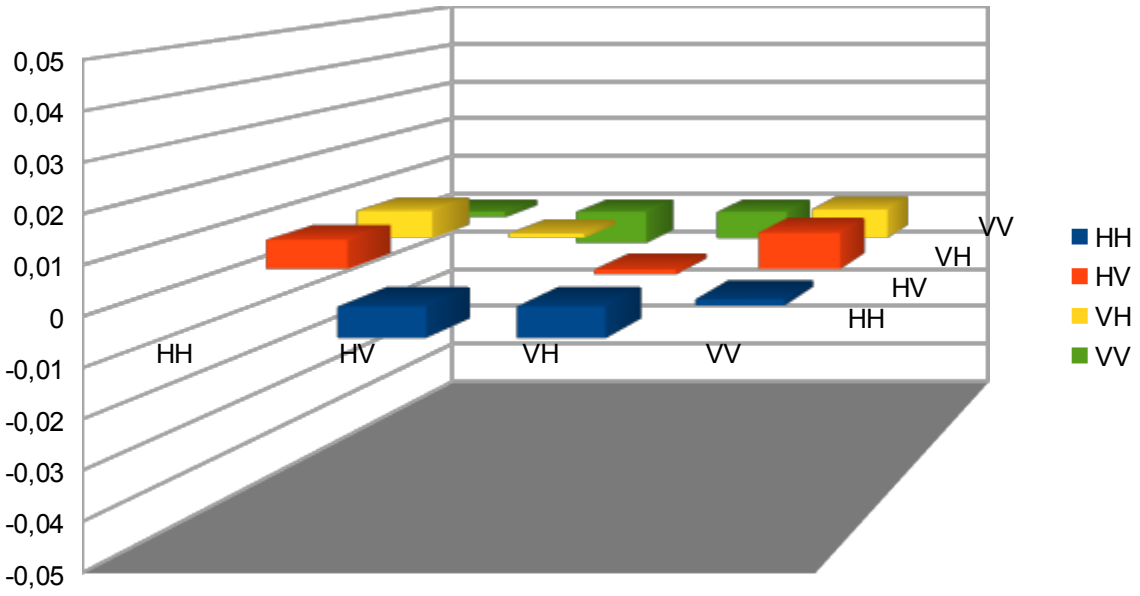

$$F_{\chi} = 0{,}988.$$

2.3 Partially tunable polarization filter

One goal of the thesis is build and characterize a tunable polarization filter. Polarization filter is an device where one or both polarization components of the laser beam are attenuated. We change linear polarization (|H>, |V>) into arbitrary linear polarization state. Polarization filter is realized by two VOD half waveplates and BD2. Our calcite displacer BD1 separates horizontal (upper path) and vertical polarization (lower path) by *4 mm*. VOD HWPs have holes which are *6 mm* wide in a diameter. So we were able to put VOD HWPs inside our interferometer so that one path interacts with HWPs and the second does not. I put one HWP into each path, see figure 12. In that way I was able to manipulate both polarizations independently by setting VOD HWPs. The actual filtering is realized by BD2. Physical implementation of the setup is shown on figure 13.

Figure 12: Tunable polarization filter.

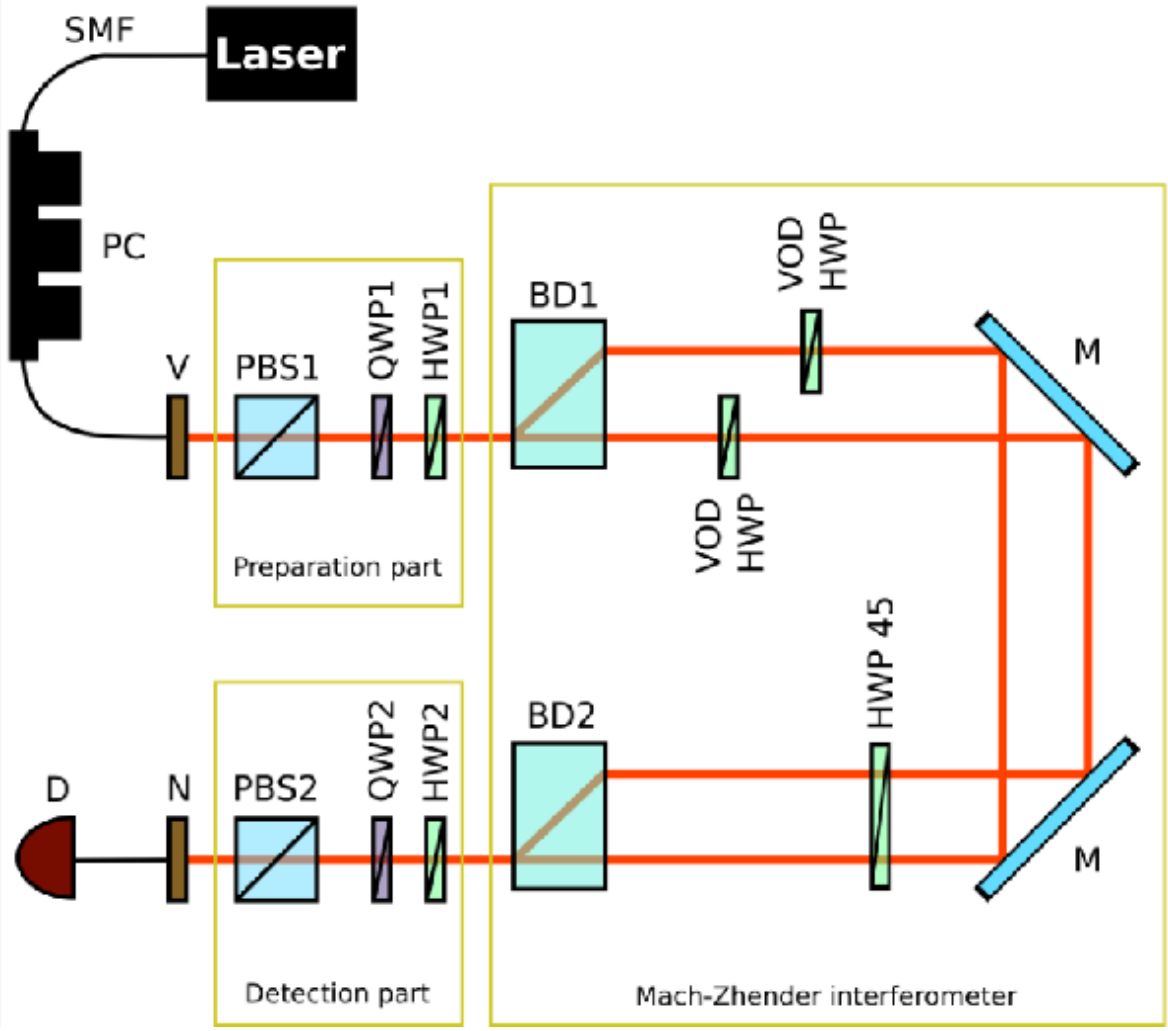

After adding VOD HWP's into experimental setup we achieved *80%* coupling efficiency to optical fiber. The measured visibility was V=*0,993*. We measured three different complete tomographies for polarization filters where the filter was set to transmit only 1/2, 1/3 and 2/3 of incident horizontal polarization. From measured data I calculated

process fidelities for all filters. Process fidelities (appendix 4) in all cases were below *0,36.* In order to obtain better process fidelities I applied to all polarization filters particular unitary operation to compensate the phase shifts, see table 9. To ilustrate 1/2 polarization filter behaviour we show reconstruced states as well as caluclated purities and fidelities on figure 14. Compensated proces matrices for 1/2, 1/3 and 2/3 filters and their theoretical process matrices are shown in figure 15, 16 and 17, respectively.

Figure 13: Physical implementation of partially tunable polarization filter. Red emphasise paths of the light.

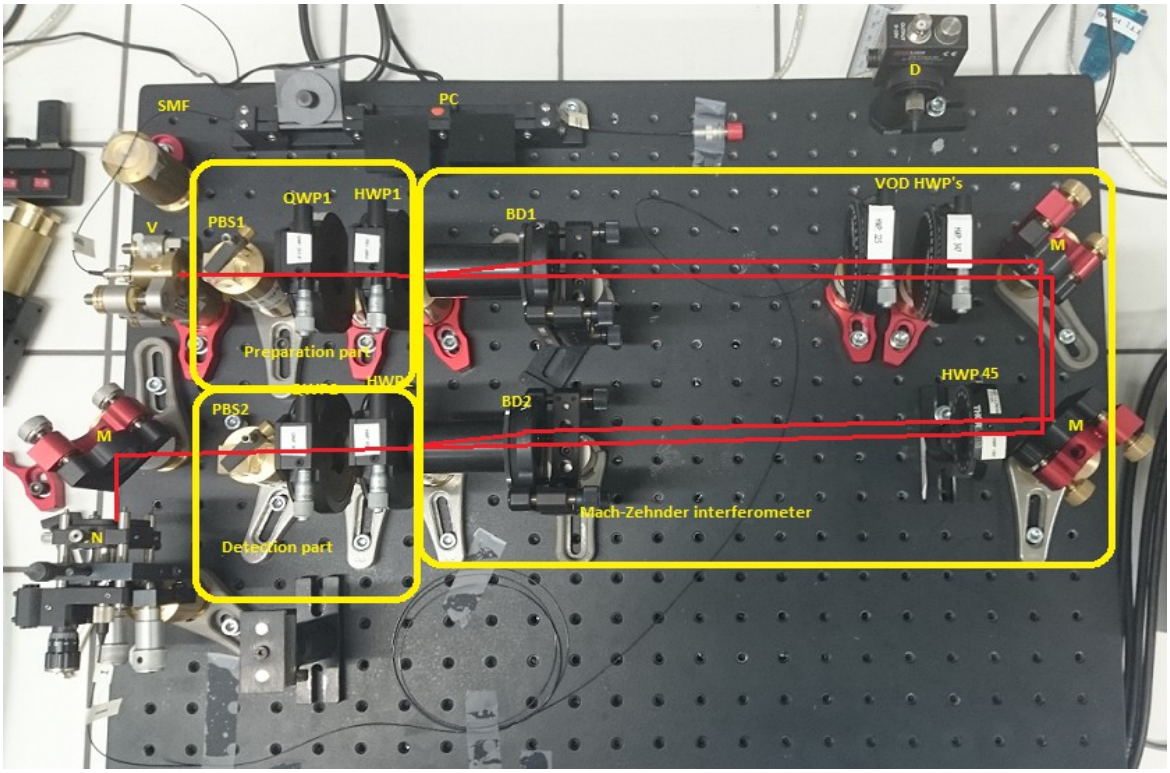

Table 9: Filter fidelities F_χ before phase compensation and F'_χ after compensation and compensating phase Φ .

Filter	F_χ	F'_χ	Φ [degrees]
$\frac{1}{2}$	0,21	0,98	160
$\frac{1}{3}$	0,36	0,96	161
$\frac{2}{3}$	0,11	0,94	203

Figure 14: Reconstructed density matrices of ½ intensity attenuator in horizontal polarizaton.

Real part of |H> polarization state.

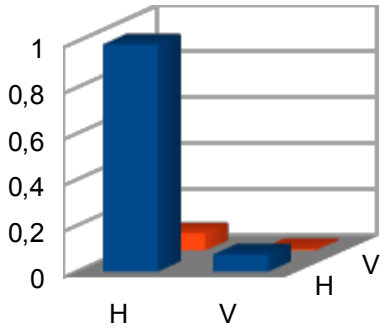

P=0,999 F=0,991

Real part of |V> polarization state.

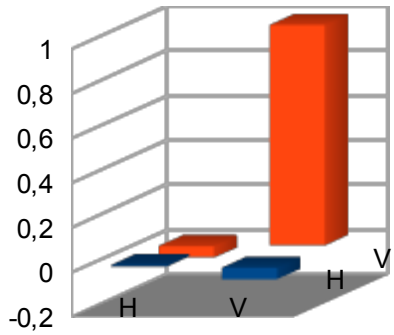

P=0,989 F=0,989

Real part of |D> polarization state.

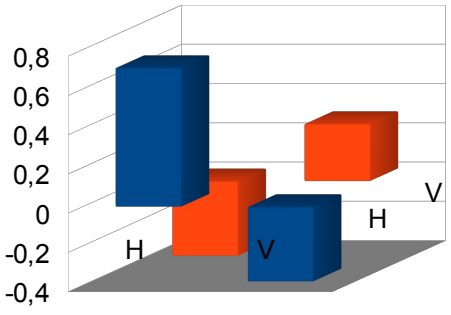

P=0,999

Imaginary part of |D> polarization state.

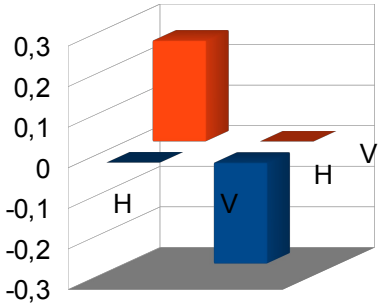

F=0,997

Real part of |A> polarization state.

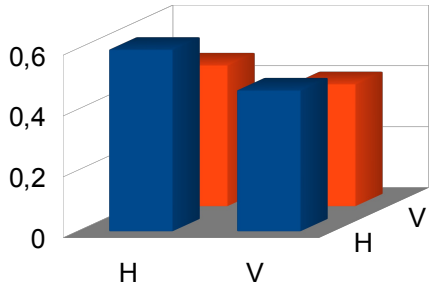

P=0,999

Imaginary part of |A> polarization state.

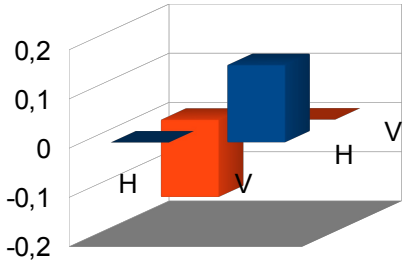

F=0,976

Real part of |R> polarization state.

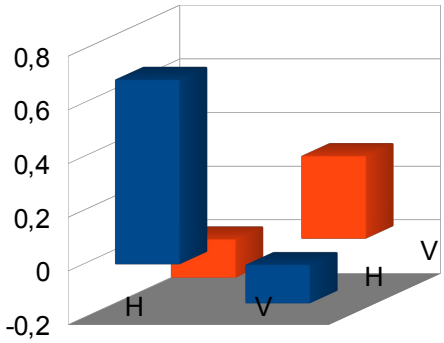

P=0,999

Imaginary part of |R> polarization state.

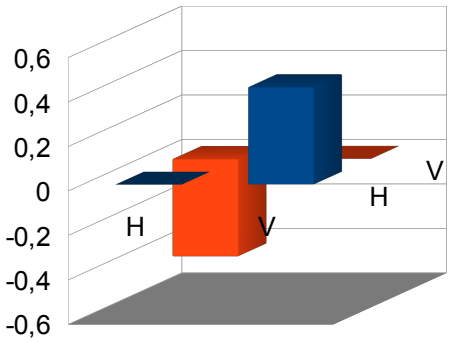

F=0,981

Real part of |L> polarization state.

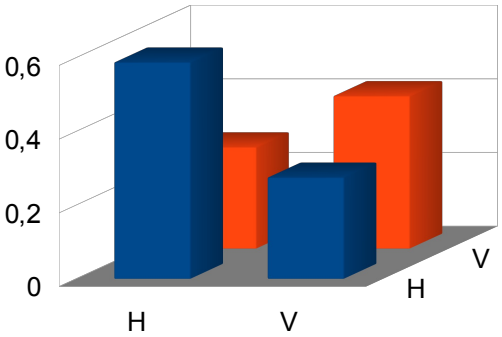

P=0,999

Imaginary part of |L> polarization state.

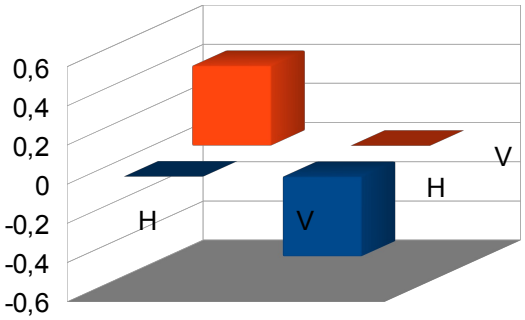

F=0,992

Figure 15: Experimental and theoretical process matrix for ½ intensity attenuator for horizontal polarization.

Real part of experimental process matrix.

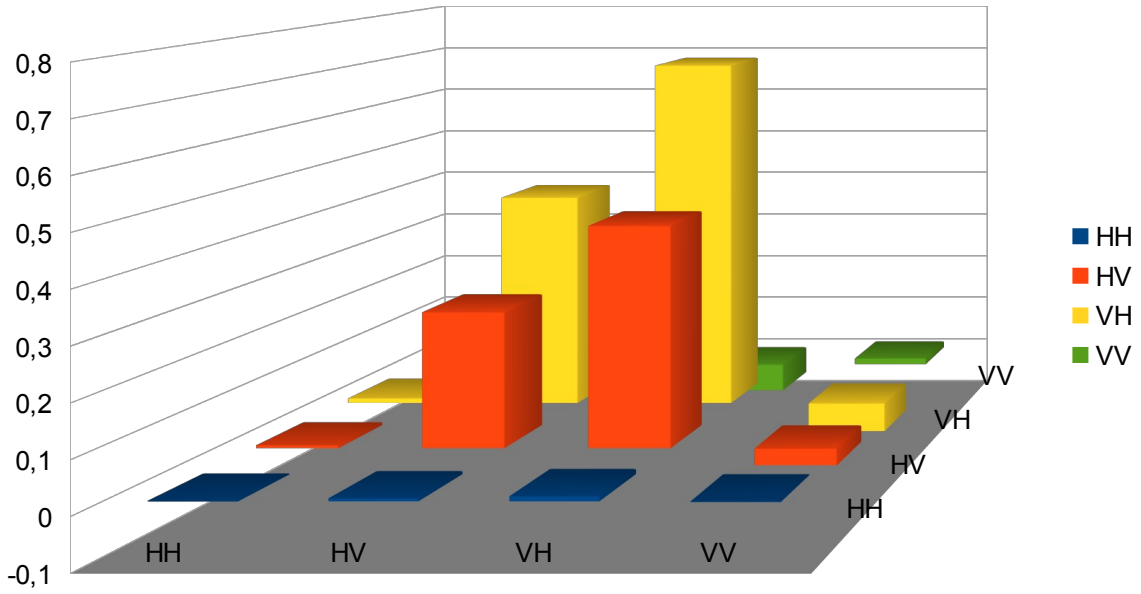

Real part of theoretical process matrix.

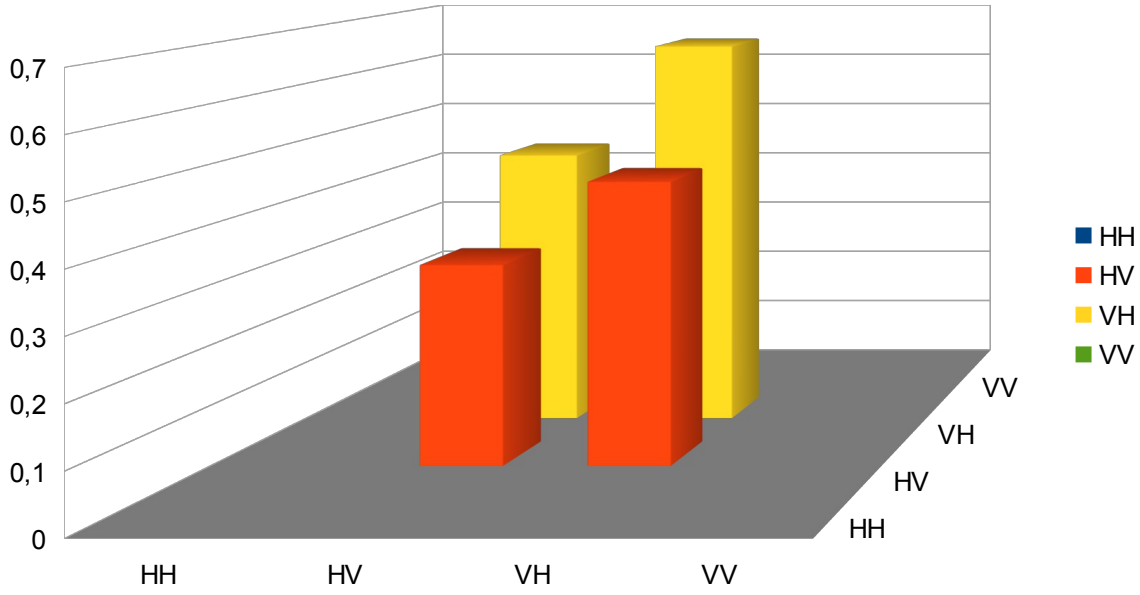

$F_{\chi} = 0{,}979$

Figure 16: Experimental and theoretical process matrix for 1/3 intensity attenuator for horizontal polarization.

Real part of experimental process matrix.

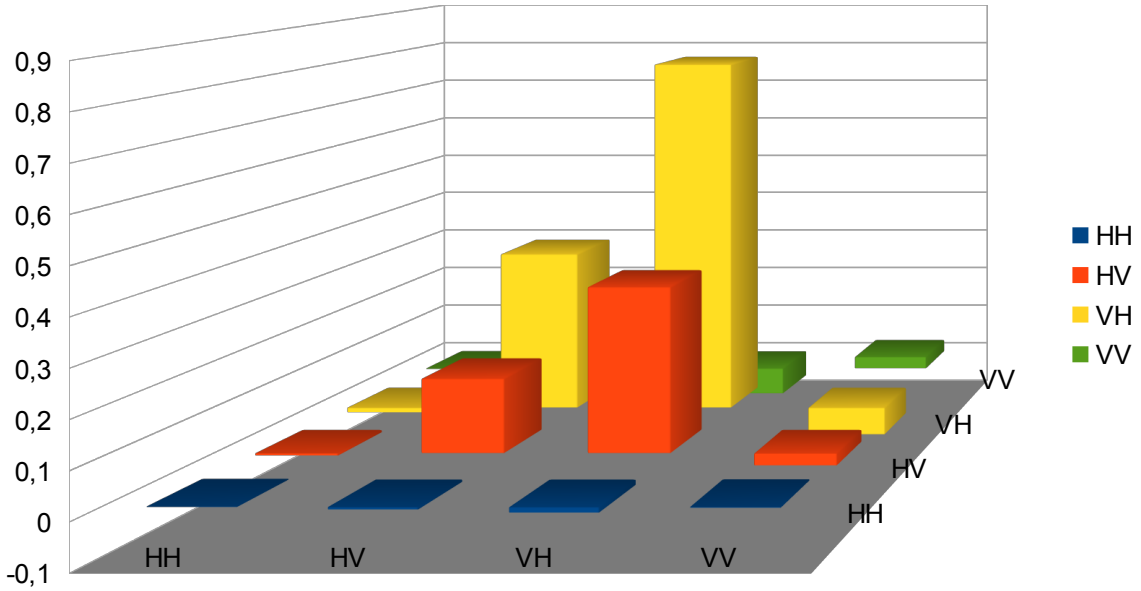

Real part of theoretical process matrix.

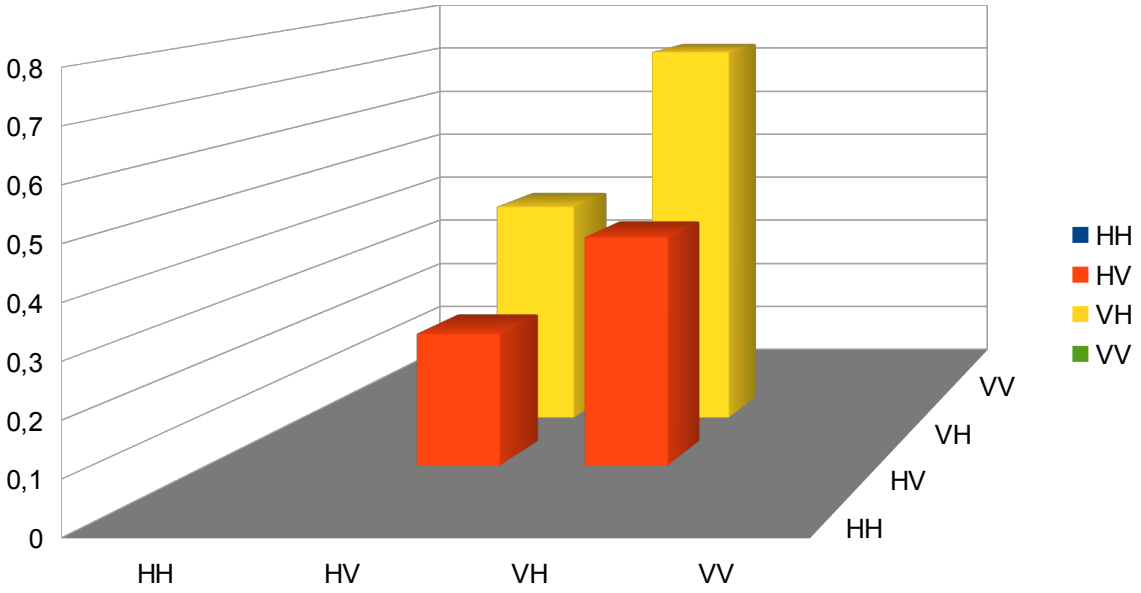

$F_{\chi} = 0{,}959$

Figure 17: Experimental and theoretical process matrix for 2/3 intensity attenuator for horizontal polarization.

Real part of experimental process matrix.

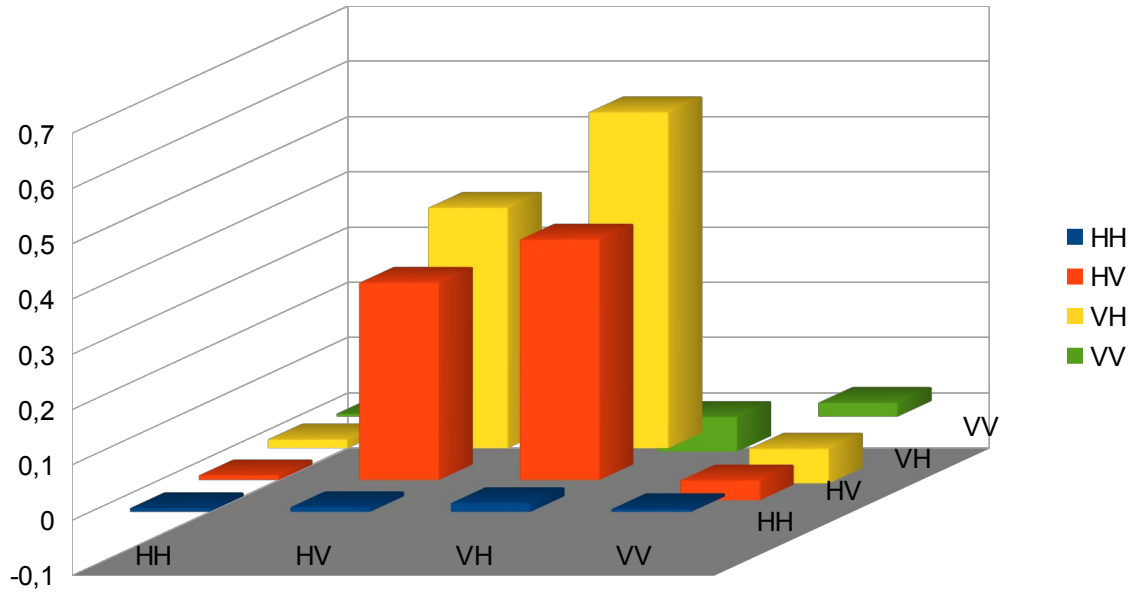

Real part of theoretical process matrix.

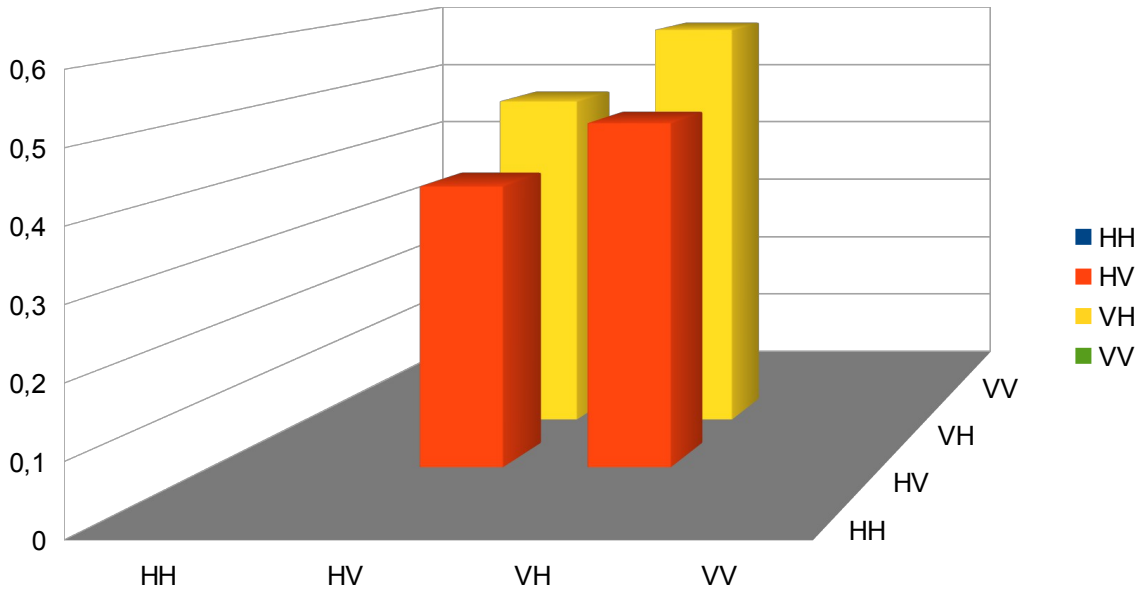

$F_{\chi}=0{,}937$

2.4 Polarization and spatial hyper-encoding

Our final experiment was dealing with encoding information in both spatial and polarization modes. In order to apply polarization coding in our experimental setup we had to add preparation and detection part of the second qubit, see figure 18. In order to characterize the device we had to realize *1296* measurements. We had to prepare six combinations of polarization on both qubits in preparation parts, which gives us thirty six combinations together. In order to collect information for state reconstruction we had to realize thirty six projections in detection part. So doing this manually would had been extremely demanding. We decided to automatize the detection part of 1st and 2nd qubit.

Figure 18: Experimental setup for spatial and polarization coding.

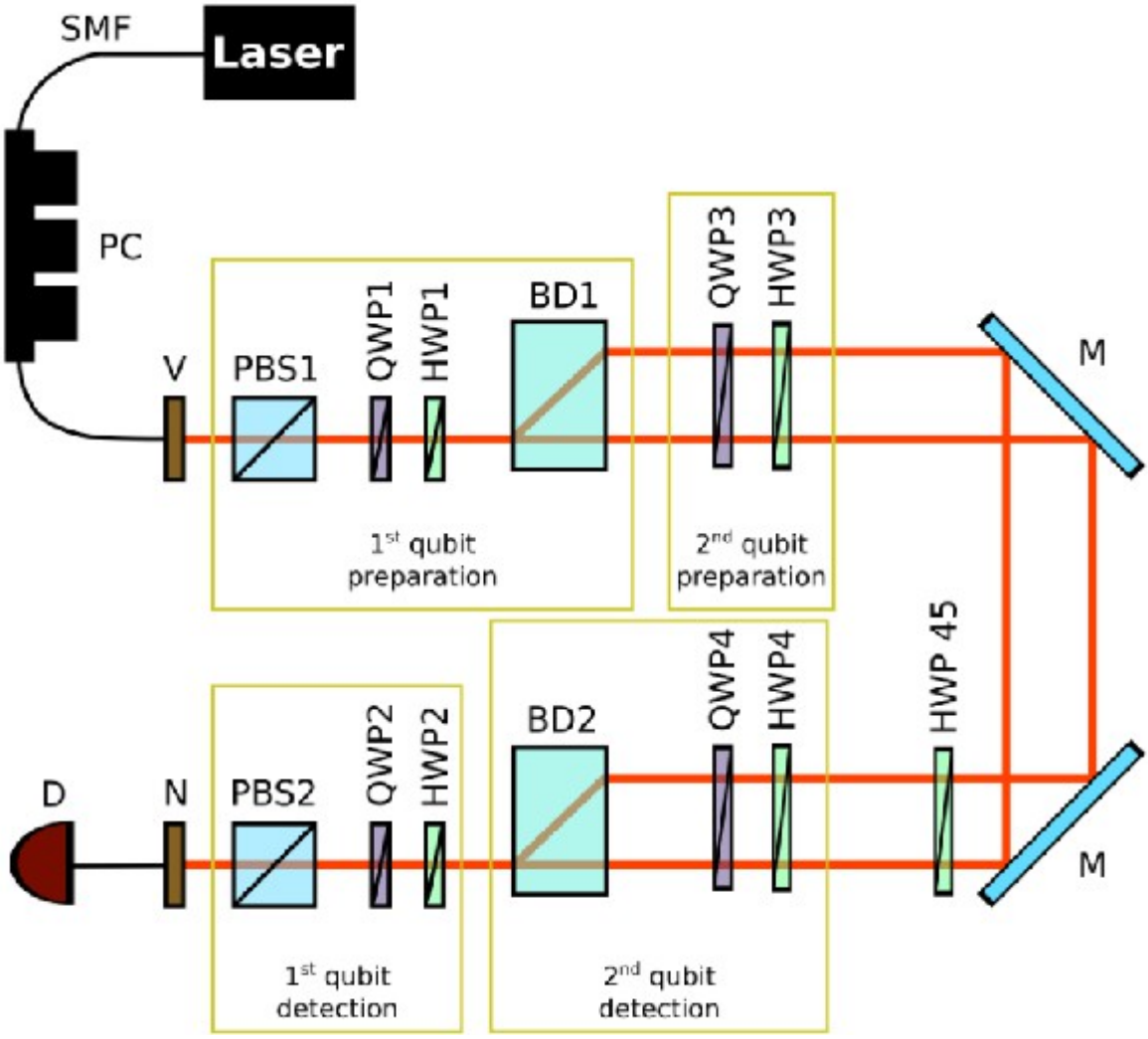

For automatization of our waveplates we put them into motorized rotation stages Newport SMC100. Since our waveplates are not calibrated I had to write a computer script for calibration. In the end we used manual waveplates for preparation parts and automatized waveplates for detection parts. Photo of experimetal realization is shown on figure 19.

To automatize motorized stages we wrote a computer script. At the beginning the waveplates rotates to |HH> position. Where on first place is detection of 1st qubit and in second place is detection of 2nd qubit. Then it measures and writes the data to a text book. Then it changes the position to |HV>, |HD>, |HA>, |HR>, |HL> where after changing every position it measures and writes down the data. This is the first cycle. After this cycle the 1st qubit in detection part changes its position to |V> polarization and 2nd qubit in detection part changes its position to |H> polarization. Data are measured, written down and the next cycle continues. There are six cycles alltogether for every input state.

We measured full tomography for this two qubit device. All states are reconstructed using maximum-likelihood method. To reach higher state fidelities we had to compensate the phase shift which we applied to measured data. Calculated purities, fidelities and phase shifts are shown table 10.

As an example, I provide reconstructed state for |HH> and |AR> polarization as well as their theoretical counterparts, see figure 18.

Figure 19: Experimentaly realized information encoding into polarization and spatial mode of light. Red lines emphasise paths of the light.

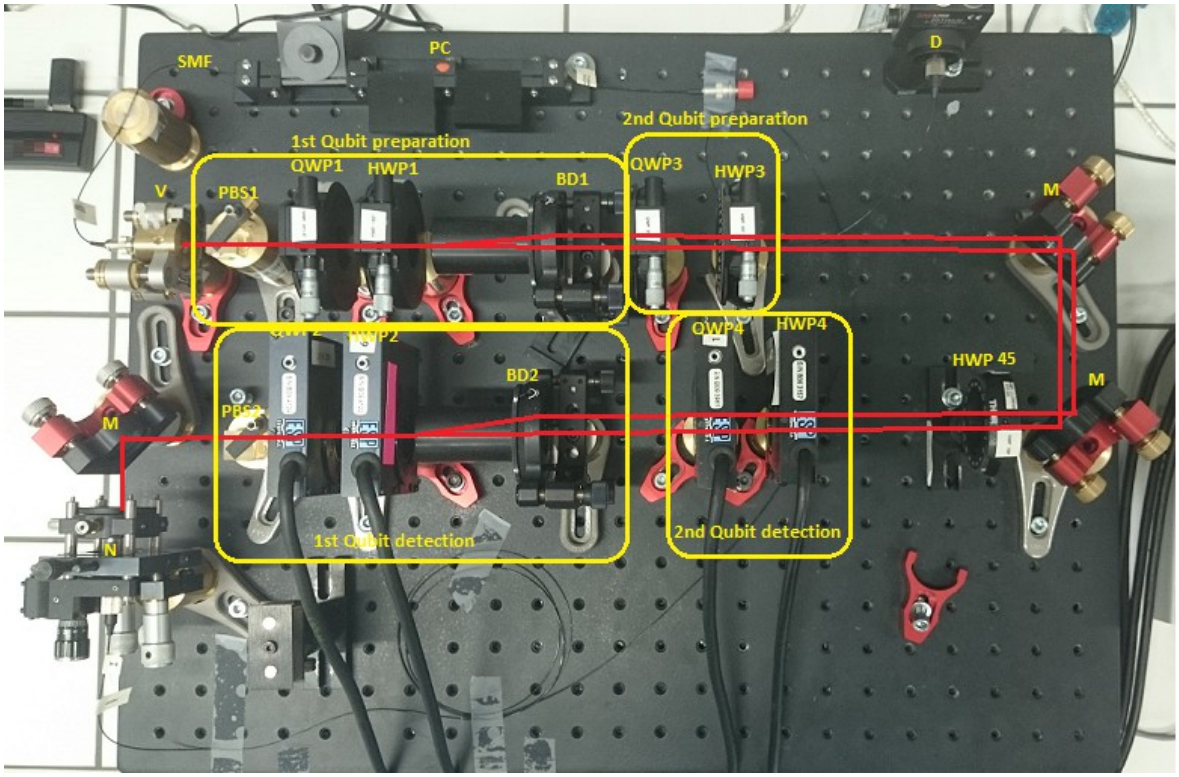

Figure 18: Reconstruction of hyper-encoded states.

Reconstructed |HH> state.

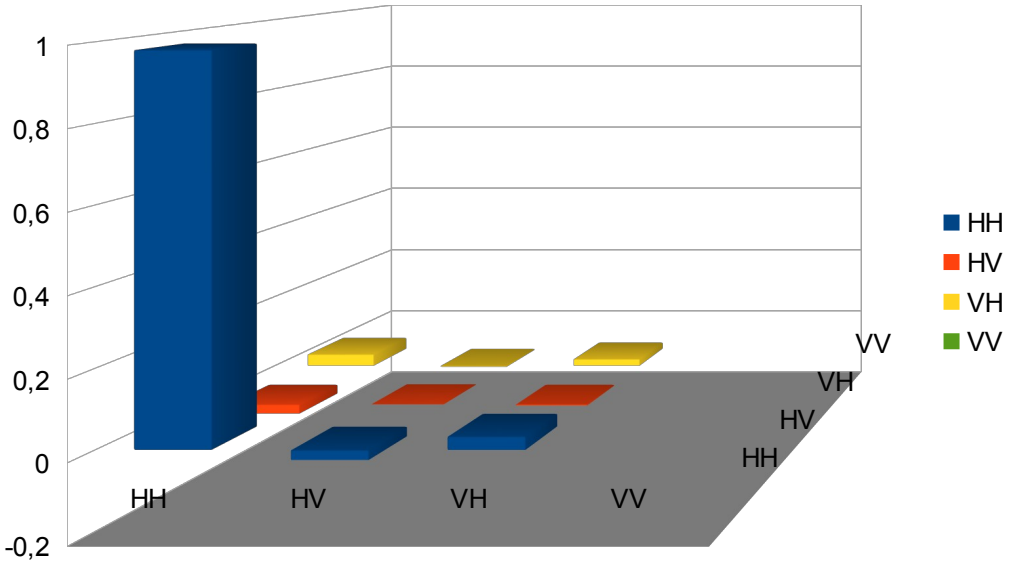

Theoretical |HH> state.

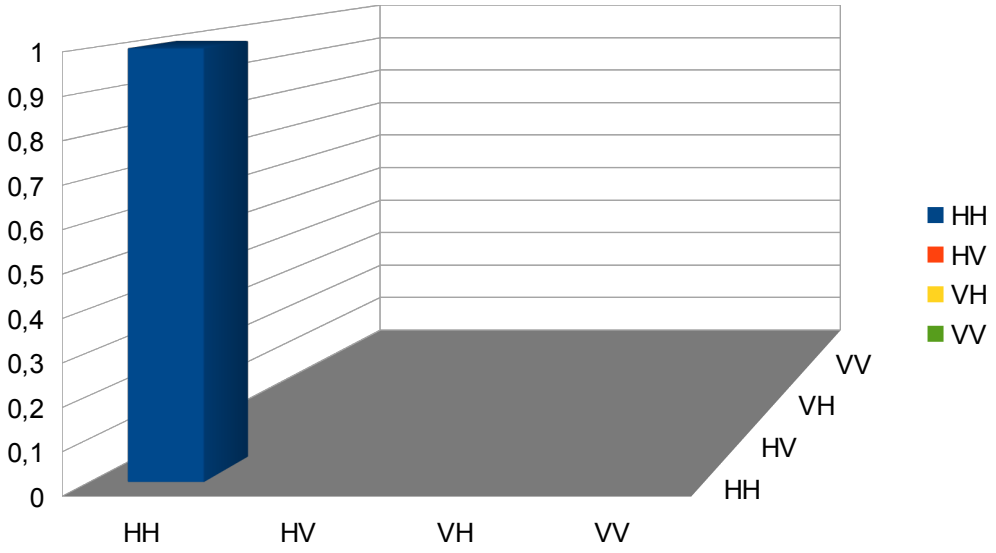

P=0,999 *F=0,979*

Real part of reconstructed |AR> state.

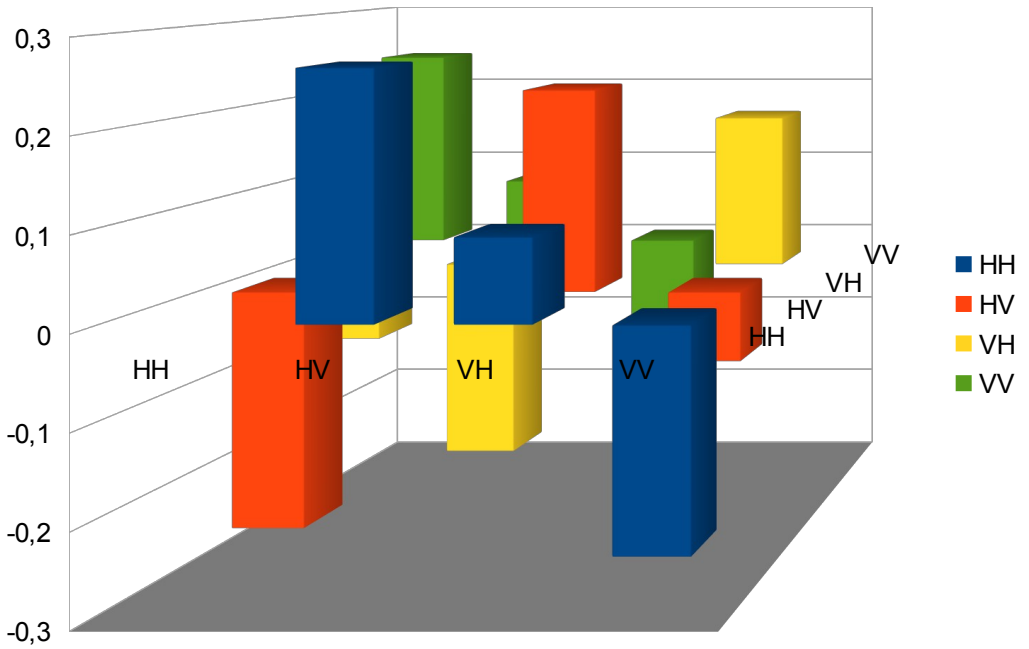

Real part of theoretical |AR> state.

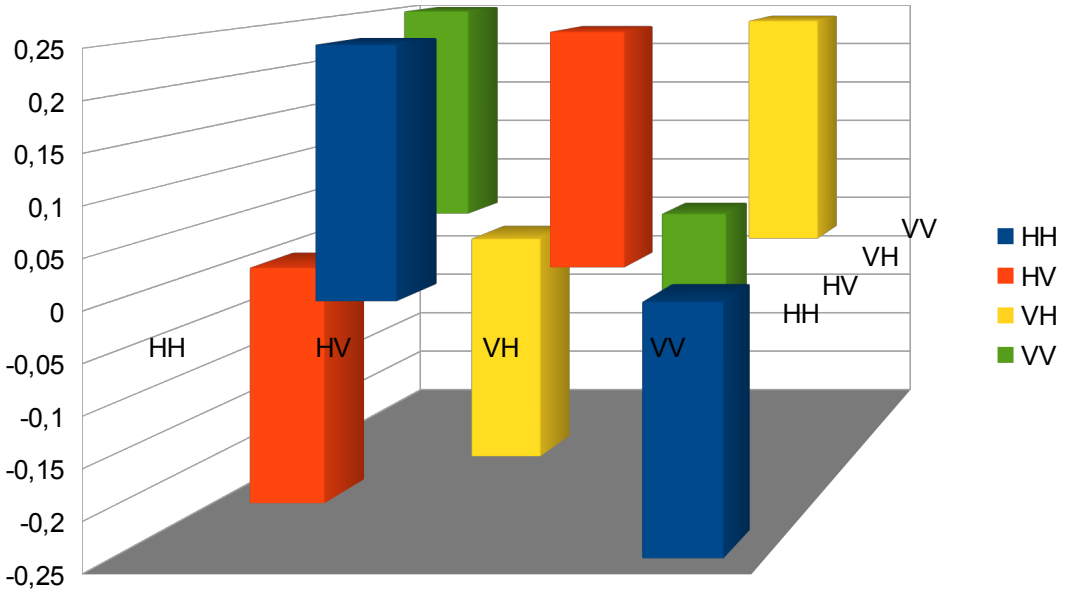

Imaginary part of reconstructed |AR> state.

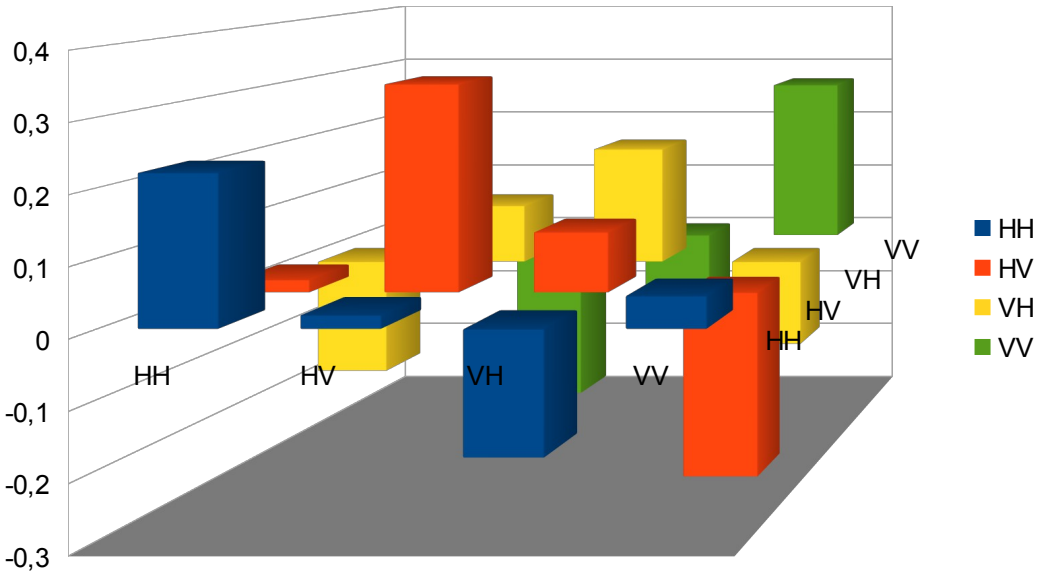

Imaginary part of theoretical |AR> state.

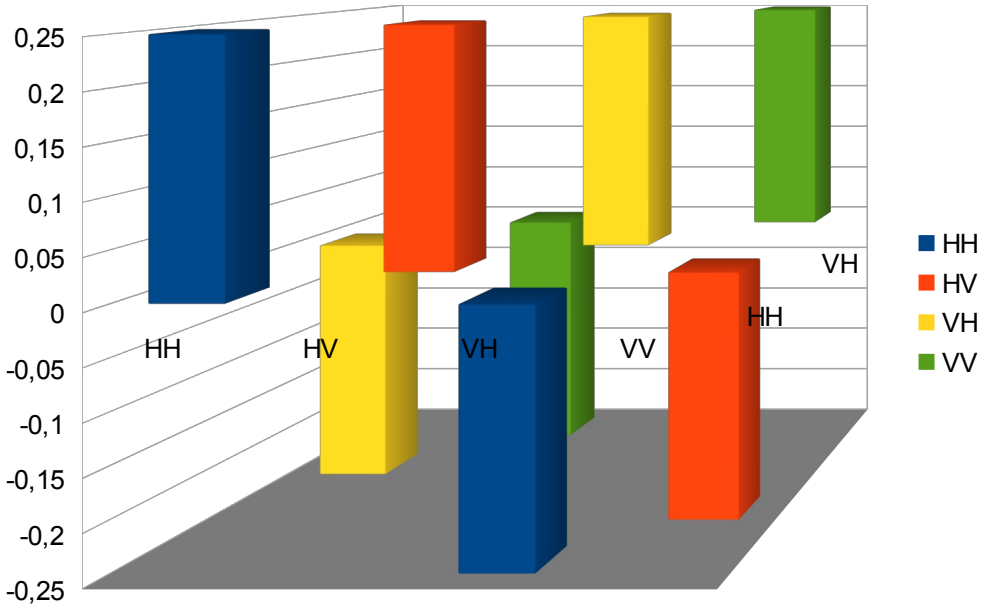

P=0,999 *F=0,939*

Table 10: Input states, reconstructed states, compensating phases Φ , fidelities F before phase compensation and F' after phase compensation, purities P.

Input state	Reconstructed state	Φ [degrees]	F	F'	P
|HH>	|HH>	0	0,979	0,979	0,999
|HV>	|HV>	0	0,979	0,979	0,999
|HD>	|HD>	0	0,979	0,979	0,999
|HA>	|HA>	0	0,949	0,949	0,999
|HR>	|HR>	0	0,977	0,977	0,999
|HL>	|HL>	0	0,996	0,996	0,999
|VH>	|VH>	0	0,979	0,000	0,999
|VV>	|VV>	0	0,951	0,951	0,999
|VD>	|VD>	0	0,979	0,979	0,999
|VA>	|VA>	0	0,999	0,999	0,999
|VR>	|VR>	0	0,949	0,949	0,999
|VL>	|VL>	0	0,964	0,964	0,999
|DH>	|DH>	0	0,991	0,991	0,999
|DV>	|DV>	225	0,146	0,988	0,999
|DD>	|DD>	200	0,042	0,805	0,999
|DA>	|DA>	155	0,039	0,918	0,740
|DR>	|DR>	-5	0,946	0,947	0,999
|DL>	|DL>	-30	0,779	0,845	0,999
|AH>	|AH>	160	0,023	0,998	0,999
|AV>	|AV>	-120	0,249	0,972	0,999
|AD>	|AD>	0	0,820	0,820	0,752
|AA>	|AA>	180	0,121	0,823	0,775
|AR>	|AR>	0	0,939	0,939	0,999
|AL>	|AL>	-40	0,655	0,696	0,999
|RH>	|RH>	-25	0,882	0,982	0,999
|RV>	|RV>	39	0,827	0,984	0,999
|RD>	|RD>	45	0,781	0,939	0,999
|RA>	|RA>	45	0,782	0,948	0,999
|RR>	|RR>	200	0,021	0,931	0,999
|RL>	|RL>	230	0,151	0,849	0,999
|LH>	|LH>	0	0,631	0,631	0,999
|LV>	|LV>	0	0,631	0,631	0,999
|LD>	|LA>	0	0,626	0,626	0,999

|LA>	|LD>	0	0,632	0,632	0,999
|LR>	|LR>	0	0,494	0,494	0,999
|LL>	|LL>	0	0,504	0,504	0,999

From table 10 we see that purities of reconstructed states |DA>, |AD> and |AA> drops to *0,745* while in others are *0,999*. We suspect that this is due phase fluctuations which have occurred during the state measurements.

Moreover we also found out that the phase differs from state to state. For example we can see this difference in state compensation between |DH> and |DV> state. Which yields *225* degrees.

Last inconsistent result with theoretical expectation are cases where we prepared left cicular polarization in the 1st qubit preparation. Although these states are pure the fidelities are below *0,632*. We were not able to compensate the global phase of the measurement states to reach higher fidelities. Unfortunatelly we do not know what caused this discrepancy between experiment and theory, yet. We plan to investigate this issue in near future.

Chapter 3

Conclusion

In the first part of my thesis we built a convertor between polarization and spatial coding. We characterized the device by one qubit reconstruction using linear inversion method. We evaluated our results with and without consideration of detectors noise. We could see that when we do not take noise detector into account, purities and fidelities of reconstructed states increased and are very close *1.* We also characterized the device by its process fidelity and it yields *0,988.*

In the next experiment we build a tunable polarization filter which attenuates one or two polarization components of laser beam. We increased the length of the Mach-Zehnder interferometer from *28 cm* to *72 cm* by adding two mirrors. Moreover we couple the output signal to single mode fibre to eliminate detector noise. We measured complete tomography of new the device without filtering any polarization. Using maximum likelihood estimation for state recostruction and we found out that mirrors introduced global phase shift. This caused the process fidelity to drop to *0,886.* By compensating the phase the process fidelity increased to *0,988.* We measured a complete tomography for 1/2, 1/3, 2/3 polarization filters. In order to obtain the highest fidelity we had to find three unitary operations which are suitable for each particular filter individualy. Estimated process fidelities for above mentioned polarization filters are *0,979, 0,959* and *0,937,* respectively.

Last experiment we were working on was device capable of encoding information into polarization and spatial degrees of freedom of light. We characterized this device by reconstruction of all *36* input states. We found out that purities in three cases were around *0,75.* We suspect that this is due phase fluctuations which have occurred during the state measurements. In other measurements the phase seems to be constant but it differs from state to state. The inconsistent results with theory occured in cases where we prepared left cicular polarization in spatial mode of preparation stage. Although purities of those states were almost one we were unable to compensate the global phase shift to reach fidelity of the state higher than *0,632.*

Appendix

1. Calibration of the quarter wave plates and half wave plates was done in respect to PBS1 and BD1. The detector was placed behind the BD1 to find such an angle for waveplate where the initial horizontally polarized light does not change its polarization state by passing through BD1. Finding it is crutial so we would be able to rotate the polarization vector on Poincare sphere from horizontal to any arbitrary polarization basis. We found this angle by rotating the waveplates and detecting the maximum intensity behind the BD1 in the horizontally polarized output (figure 3).

Figure 3: Calibration of waveplates.

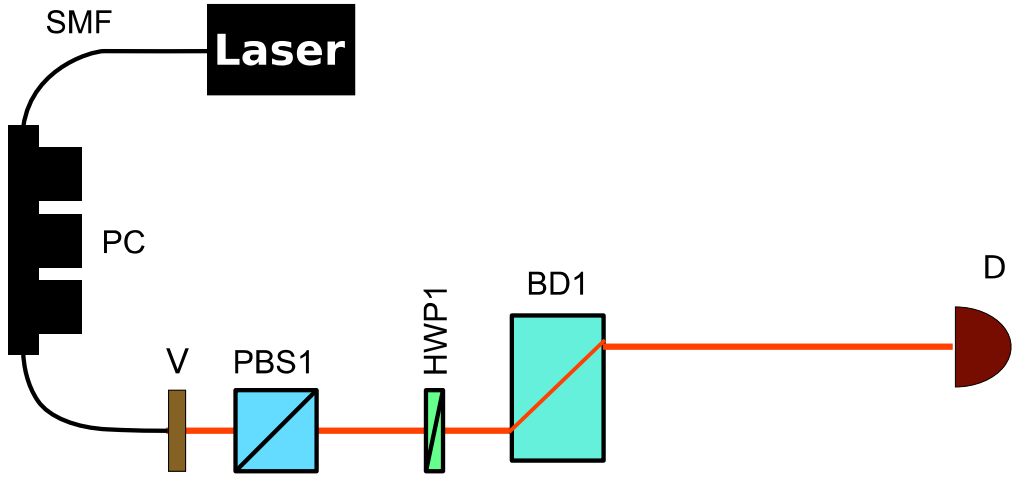

2. All the preparation parts consists off QWP and HWP, respectivelly. Horizontal polarized beam enters the quarter and half wave plate for the polarization preparation of the photons. Using this preparation setup we could rotate the vector of polarization under its axis of *x-y* which then changes the type of polarization from horizontal to vertical, diagonal, anti-diagonal, left circular, right circular and elliptical polarization, $|H\rangle,|V\rangle,|D\rangle,|A\rangle,|R\rangle,|L\rangle$ respectively. On table 11 are shown the degrees how to set up QWP1 and HWP1 in our experimental polarization preparation set up to get any arbitrary polarization basis. Degrees are written in respect to zero point of the waveplate.

Table 11: Polarization preparation for initial horizontal polarization.

	QWP [degrees]	*HWP [degrees]*
|H>	0	0
|V>	0	45
|D>	0	22,5
|A>	0	-22,5
|R>	45	0
|L>	-45	0

For detection part we placed HWP and QWP , respectively. On table 12 are shown the degrees how to set up HWP and QWP in our detection set up to measure in particular projection.

Table 12: Polarization preparation for initial horizontal polarization.

	HWP [degrees]	***QWP [degrees]***
|H>	0	0
|V>	45	0
|D>	22,5	0
|A>	-22,5	0
|R>	0	45
|L>	0	-45

3. Correcting the global phase shift is realized by finding a unitary transformation defined by matrix

$$U(\phi)=\begin{pmatrix}1 & 0\\ 0 & \exp(-i\phi)\end{pmatrix}.$$

I found a unitary operation that corrects our phase shift. Applying this matrix will correct our results. Transformation by unitary matrix is defined

$$\rho_{out}=U_T\,\rho\,U_T^{+},$$

where ρ is our reconstructed matrix, U_T^{+} is hermitian conjugate of unitary operation U^{+}.

4. Theoretical model described in this case is a little bit different than in appendix 3. The intensity attenuator is a non-unitary operation. This means our transformation through Mach-Zehnder interferometer is non-unitary

$$\rho_{ideal}=\frac{N_T\,\rho_{in}\,N_T^{+}}{Tr[N_T\,\rho\,N_T^{+}]},$$

where N_T is a non-unitary transformation, N_T^{+} is its hermitian conjugate and ρ_{in} is input state . In our case N_T is defined as

$$N_T=P_F T_1 U_T$$

where P_F is matrix which defines intensity attenuator in horizontal polarization, T_1 is matrix which defines half wave plate set on *45* degrees. Calculated fidelities are

$$F(\rho_{ideal},\rho)=Tr\{[(\rho)^{1/2}\,\rho_{ideal}\,(\rho)^{1/2}]^{1/2}\}^2 \quad ,$$

is density matrix through transformation of our system and ρ is reconstructed matrix from data.where ρ_{ideal}

References:

[1] J. L. O'Brien, G. J. Pryde, A. G. White, T. C. Ralph & D. Branning Demonstration of all-optical quantum controlled-NOT gate, Nature 426, (2003).

[2] R. Okamoto, H. F. Hofmann, S. Takeuchi & K. Sasaki Demonstration of an Optical Quantum Controlled-NOT Gate without Path Interference, Phys. Rev. Letters 95, 210506 (2005)

[3] J. B. Altepeter, E. R. Jeffrey, and P. G. Kwiat, Photonic State Tomography (Urbana IL 61801).

[4] M. Ježek, J. Fiurášek, and Z. Hradil, Quantum inference of states and processes, Phys. Rev. A 68, 012305 (2003).

[5] Saleh, Teich, Fundamentals of Photonics 1st ed 1991

[6] M. A. Nielsen, I. L. Chuang, Quantum Computation and Quantum Information (Cambridge Univ. Press, 2000).

[7] D. F. V. James, P. G. Kwiat, W. J. Munro, and A. G. White, Measurement of qubits, Phys. Rev. A 64, 052312 (2001).

[8] M. G. A. Paris, J. Řeháček, Quantum State Estimation (Springer, 2004).

[9] M. Fox, Quantum Optics (Oxford Univ. Press, 2006).

[10] S. Huard, Polarization of Light, John Wiley & Sons Ltd (1997)

[11] T. D. Ladd, F. Jelezko, R. Laflamme, Y. Nakura, C. Monroe & J. L. O'Brien Quantum Computers, Nature 464, 08812 (2010).

[12] J. L. O'Brien Optical Quantum Computing, Science 318, 1567 (2007).